

An Evaluation of the Efficacy of Very High Resolution Air-Quality Modelling over the Athabasca Oil Sands Region, Alberta, Canada

Matthew Russell¹, Amir Hakami¹, Paul A. Makar², Ayodeji Akingunola², Junhua Zhang², Michael D. Moran², and Qiong Zheng²

¹Department of Civil and Environmental Engineering, Carleton University, Ottawa, Canada

²Air Quality Research Division, Environment and Climate Change Canada, Toronto, Canada

Abstract

We examine the potential benefits of very high resolution for air-quality forecast simulations using a nested system of the Global Environmental Multiscale – Modelling Air-quality and Chemistry chemical transport model. We focus on simulations at 1km and 2.5km grid-cell spacing for the same time period and domain (the industrial emissions region of the Athabasca Oil Sands). Standard grid cell to observation station pair analyses show no benefit to the higher resolution simulation (and a degradation of performance for most metrics using this standard form of evaluation). However, when the evaluation methodology is modified, to include a search over equivalent representative regions surrounding the observation locations for the closest fit to the observations, the model simulation with the smaller grid cell size had the better performance. While other sources of model error thus dominate net performance at these two resolutions, obscuring the potential benefits of higher resolution modelling for forecasting purposes, the higher resolution simulation shows promise in terms of better aiding localized chemical analysis of pollutant plumes, through better representation of plume maxima.

1 Introduction

Numerical modeling of the atmosphere in an Eulerian framework relies on discretization of the computational domain into a numerical grid. The horizontal grid cell size of atmospheric simulations can range from hundreds of kilometers, to the metre-scale of Large Eddy Simulation models. Air-quality model grid-cell size typically follows the grid-cell sizes used in weather forecasting models, which in turn have followed a gradual progression towards finer discretization where more explicit representation of cloud formation and local radiative transfer effects may be represented. The most recent weather forecasting applications (e.g. Leroyer *et al.*, 2014) have reached grid-cell sizes as small as 250m over limited domains such as individual cities, and have shown promising results in terms of being able to resolve some aspects of local circulation. In addition, as grid resolution reaches the 3 to 4 km scale, explicit cloud microphysics packages may be used, allowing potentially better performance, particularly with regards to feedbacks between meteorology and chemistry (Yu *et al.*, 2014; Gong *et al.*, 2015). However, while these models promise better physical representation of local chemistry, their performance may be limited by the quantity and availability of initialization and boundary condition meteorological data; these data may be used in a data assimilation context to improve their initial state. The accuracy of broader-scale meteorological

34 predictions may thus influence local model accuracy, despite the ongoing decrease in meteorological model (and
35 consequently air-quality model) grid cell size. Some recent air-quality model simulation studies with grid cell sizes
36 on the order of one to four km include Thompson and Selin (2012), Li *et al.* (2014), Joe *et al.* (2014), Kheirbek *et al.*
37 (2014), Kheirbek *et al.* (2016), and Pan *et al.*, (2017).

38 For the purposes of this study, Very High Resolution (VHR) modelling refers to the current higher resolution limits
39 of chemical transport models (CTMs), employing a horizontal grid cell spacing of 1km or less. It is in this regime
40 that the photochemical processes may be forecasted with resolved microphysics (e.g. Milbrandt and Yau,
41 2005(a,b)), and detailed particle and gas-phase chemistry, using currently available computer technology. VHR
42 modelling is very computationally expensive, and also introduces its own set of challenges, such as the availability
43 of surface boundary condition fields as the model grid cell size decreases. Moreover, it is not currently clear
44 whether decreases in model grid cell size leads to more accurate results when compared to observations. The
45 motivation behind VHR modelling in CTMs is to reduce the impact of diluting chemical concentrations - especially
46 from averaging emission plumes into large grid cells – in order to better capture inhomogeneities in emission
47 profiles, to better simulate local transport processes associated with terrain that would otherwise be smoothed by
48 the use of a coarse grid, and to reduce truncation errors and hence achieve better numerical accuracy (Jacobson,
49 1999).

50 We note here that while the terms “grid cell size” and “resolution” tend to be used interchangeably in the
51 literature, this is not true in a precise mathematical sense; more formally, the ability to resolve features of size
52 $2\Delta x$ requires a grid cell spacing of size Δx , and the highest spatial frequency which can be reconstructed from a
53 discrete sampling of the latter grid cell spacing will be $\frac{1}{2\Delta x}$, the Nyquist wavenumber of the grid cell size
54 discretization. Furthermore, atmospheric models may make use of energy dissipation techniques that broaden
55 the size of resolvable wavelengths to $3\Delta x$ to $4\Delta x$ (Grasso, 2000; Pielke, 2001). Model resolution is thus a function
56 of, but not equivalent to, grid cell size. Here, we define “resolution” as the ability of a model to clearly distinguish
57 components of a predicted atmospheric variable, as a *function* of grid cell size.

58 The issue of a model to distinguish these features is also compounded by uncertainties in model inputs. For
59 example, in a large rural setting, a large model grid cell will represent an area containing many roads, whose
60 emissions will be averaged into one value per species per time. As the grid cell size decreases however, this
61 averaging effect will be reduced, giving each road’s emissions more impact on the resulting concentrations in the
62 grid cell containing it. However, the smaller grid cell size will also result in steeper concentration gradients in the
63 model between adjacent grid cells, which can in turn result in numerical instabilities that contaminate predictions
64 (Salvador *et al.*, 1999). At the same time, a reduction in grid-cell size can be shown formally to reduce
65 inaccuracies in the discretization of the governing equations for atmospheric motion (Coiffier, 2011). Previous
66 efforts to address these issues through variable grid size or structure in air quality modeling have not received

67 sustained attention, and therefore most current air quality models use a uniform (albeit nested) grid cell size in
68 applications (Garcia-Menendez *et al.*, 2010; Kumar *et al.*, 1997).

69 As resolution increases further, the presence of local topographical features (*e.g.* buildings and street canyons)
70 become more important. Both the increased topographic complexity, and potential numerical instabilities can
71 lead to differences in meteorological forcing as resolution increases (Wolke, *et al.*, 2012; Gego, *et al.*, 2005)). The
72 contribution of meteorological uncertainties due to resolution become more significant, especially for secondary
73 pollutants such as ozone (Valari and Menut, 2008) or secondary Particulate Matter (PM). For example, Markakis *et al.*
74 *al.* (2015) in their analysis of 4 km CHIMERE simulations for the relatively flat terrain of Paris, France, suggested
75 that model meteorological grid cell size does not significantly impact forecast accuracy. That may not have been
76 the case, had their terrain been more complex. In contrast, Queen and Zhang (2008) observed considerable
77 meteorological sensitivity to the more complex terrain in their 4 km resolution Community Multiscale Air Quality
78 (CMAQ, EPA 1999) model simulations over the Appalachian Mountains in the eastern United States, as did
79 Salvador *et al.* (1999) for meteorological model simulations.

80 A number of studies have tried to evaluate the benefits of higher resolution simulations and to quantify the
81 impact of sub-grid variability by using different model grid-cell sizes (Vardoulakis *et al.*, 2003; Ching *et al.*, 2006;
82 Pepe *et al.*, 2016). These studies have often demonstrated that failure to account for higher resolution features
83 may result in mischaracterization of concentrations or health impacts (Isakov *et al.*, 2007), although the capability
84 of current models to provide this information with sufficient accuracy is unclear. One study found that increasing
85 resolution did not change predicted health outcomes, and concluded that “resolution requirements should be
86 assessed on a case-by-case basis” (Thompson and Selin, 2012), while others (*e.g.* Kheirbek *et al.* (2014), Kheirbek
87 *et al.* (2016)) have employed 1km resolution without discussing the impacts of resolution on predicted health
88 outcomes. Population exposure studies using air pollution models may be affected by resolution in a more
89 complex fashion, given that both the predicted field (a pollutant with a known health impact) and the data to
90 which the predicted field is to be linked (the human population) both have resolution dependencies. The health
91 studies carried out to date highlight the need for better understanding the underlying controlling factors for
92 model accuracy with decreasing grid cell size.

93 Terrain and meteorology are not the only factors that contribute to greater uncertainties as horizontal grid cell
94 size is reduced – for example, the ability of the model to locally resolve emission fluxes may also become a factor.
95 This may result in improved or deteriorated model performance as the size of the grid cells decrease. Gridded
96 model emissions may have an intrinsic resolution dependence in the underlying spatial disaggregation fields, and
97 this can contribute to uncertainties and errors in emissions as grid cell size is decreased. For instance, Valari and
98 Menut (2008) found that the discrepancy between their modelled and observed concentrations grew, rather than
99 shrank, in response to decreases in grid cell size from 48km to 6 km, and they associated these results with

100 changes in the resulting local emission fluxes. They showed that in their model setup, with regard to ozone, a grid
101 cell size was reached (12x12 km²) where errors in inputs (errors in the emission inventory, wind direction, etc.)
102 outweighed the importance of other sources of model error such as grid cell size. The authors however noted that
103 Paris' ozone photochemistry very often resides on the transition between a NO_x-sensitive and a VOC-sensitive
104 regime (Sillman *et al.*, 2003). These are chemical conditions which can alternatively produce or titrate ozone, and
105 hence have a degree of sensitivity to precursor emissions, and therefore, also, to any errors in those emissions.
106 Conversely, in a 3-level nested 9- to 3- to 1- km MM5-CMAQ simulation over Osaka, Japan, Shrestha *et al.*, (2009)
107 found that ozone comparisons to observations improved as the grid resolution increased. This was also the case
108 for a 36- to 12- to 4-km nested MM5-CMAQ simulation over Houston, USA (Ching *et al.*, 2006), where the ozone
109 forecast improvement associated with higher resolution was attributed to the ability of the finer grid cell size
110 model nests to adequately resolve high concentrations of freshly emitted NO_x and hence allow for more local
111 ozone titration. The latter process might not take effect until the grid cell size is sufficiently fine to resolve the NO_x
112 source patterns (*i.e.*, a level where traffic and industrial sources can be identified.) This titration was not seen until
113 they decreased their grid cell sizes to 2 km and smaller. Stroud *et al.* (2011) noted a similar grid cell size
114 dependent chemical impact on model performance, where secondary organic aerosol formation maxima were
115 better simulated with a 2.5km grid cell size model than a 10km grid cell size model. In general, the impact of
116 resolution on model performance appears to depend on a number of factors, such as the terrain, spatial
117 distribution of sources, pollutant of concern, season, etc. (Arunachalam *et al.*, 2006; Queen and Zhang, 2008; Dore
118 *et al.*, 2012).

119 Salvador *et al.* (1999) studied the prediction accuracy impacts of meteorological model grid cell size in a region
120 with complex domain, and found that 2km or smaller grid cell sizes were required to resolve local scale complex
121 terrain flow features, and that daytime vertical advection and predictions of turbulent kinetic energy and potential
122 temperature were influenced by grid cell size. Dore *et al.* (2012) evaluated air quality model NO₂ simulations
123 employing 1, 5 and 50km grid cell sizes against observations, and found the best performance for the 1km
124 simulation, with more physically realistic distributions of reactive nitrogen, attributing this performance gain to
125 more realistically precipitation simulations and emissions inputs for the smallest grid cell size. The availability of
126 high-resolution emissions information may be a limiting factor in improved simulations as grid cell size decreases.
127 Valari and Menut (2008) noted that emissions inaccuracy was the principal cause of noise in small grid cell size
128 simulations conducted for the Paris area, and proposed the use of statistical downscaling in favour of predictive
129 modelling at scales at or below 1km grid cell size. The current state of model science is typically evaluated
130 through multi-model intercomparisons (e.g. Im *et al.*, 2015), and the meta-analysis of these studies can be used to
131 provide useful benchmarks to assess current model performance for specific model species and observations
132 (Emery *et al.*, 2017). However, such studies do not identify the causes for good or poor performance relative to
133 the benchmarks – diagnostic studies, “in which chemical and physical processes within the model are analyzed

134 individually and collectively” (Emery *et al.*, 2017) are required for this purpose. Examinations of the impact of
135 model grid cell size on performance are an example of such a diagnostic evaluation.

136 The benefits for model performance with increased spatial resolution are unclear, based on the above literature.
137 However, most papers converge towards the following qualitative conclusions:

- 138 1. The impact of terrain topology on meteorological forcing as grid cell size decreases can dwarf the impact of
139 a more accurate spatial apportionment of the corresponding emissions.
- 140 2. Decreases in grid cell size result in a more realistic spatial distribution of chemical species, whether or not
141 model performance is improved.
- 142 3. Uncertainties of spatial and temporal emissions allocation have an increasing influence on overall model
143 uncertainty as model grid cell size decreases.

144 The 1980’s saw several studies in which the potential impacts of wind direction errors on dispersion model
145 performance were examined. Fox (1981) noted that pairing of model output at observation station locations could
146 be done as a function of both time and space: as a function of time (by combining the data across all stations), as a
147 function of space (by combining all times, at each station location), or without any pairing (observations and data
148 were compared as cumulative frequency distributions). The accuracy of regulatory dispersion models in the early
149 1980’s was such that Fox (1984) concluded that model and observation values paired in time and space exhibited
150 “little to no correlation” and discussed potential errors associated with transport. Poor correlations were also
151 noted by Hanha (1988), reporting on the first generation of reactive-transport models, stated “wind direction errors
152 are the major cause of the poor agreement in hourly predictions of concentrations at short distances downwind of
153 point sources,” as well as describing metrics for air-quality model evaluation. Hanha (1988) also noted that model
154 predictions could be offset in space and time relative to observations, leading to poor performance statistics,
155 despite a greater degree of similarity of behavior if the offsets are taken into account. Errors in wind-field
156 modelling were described as the main source of error in simulations of plumes by Carhart *et al* (1989), again
157 showing how better agreement resulted when model and observations were unpaired in time and/or space, and
158 noted that other metrics such as maximum plume width might better represent model performance. Lee (1987)
159 found that small perturbations in space and time could result in poor correlations, despite similar histogram
160 distributions of both model and observations.

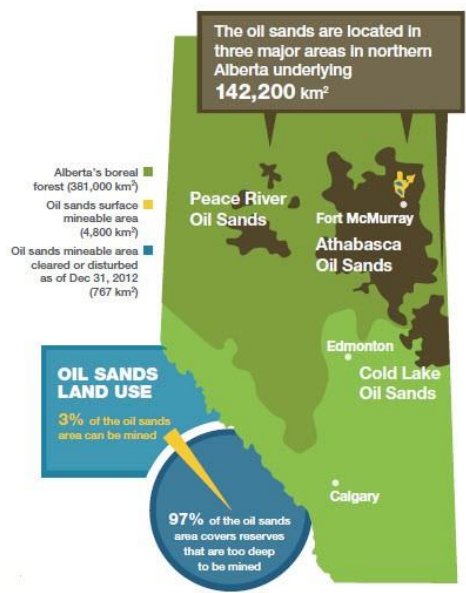
161 More recently, Kang *et al.*, (2007) examined the concept of using the area of the limiting resolution of the model (2
162 to $3\Delta x$, where Δx is the horizontal grid cell size) to weight or spatially average model evaluation metrics for a single
163 grid-cell size, noting how the model’s rated ability to capture high concentration events (“hits”) was increased when
164 the limiting resolution of the model was incorporated into the performance metrics. However, the use of averaging
165 may mask the potential for a model with a small grid cell size to contain both the desired plume magnitude, as well

166 as much lower concentrations, within the same larger representative area, in turn masking the potential impact of
167 the reduction in grid cell size.

168 We expand on this concept to evaluate the impact of model grid cell size in the context of an equivalent area about
169 a given observation location. We examine area-weighted metrics in the form of averages over roughly equivalent
170 areas for different model grid cell sizes, and also use the *a priori* knowledge of the observations to determine
171 whether the closest match to observations may be found within an equivalent area. We show that the latter metric
172 demonstrates a positive impact of model grid cell size on simulation results, while more simple paired comparisons,
173 and averages over similar areas, mask these benefits.

174 We examine the impact of grid cell size on model performance in a region of intense petrochemical extraction and
175 upgrading, the Athabasca Oil Sands Region (AOSR). The AOSR refers to the northernmost of three large bitumen
176 deposits located the northern part of the province of Alberta in Canada; the Athabasca, Peace River, and Cold Lake
177 areas. Together these areas cover 142,200 km² in total, and constitute the third largest oil reserves in the world
178 (Government of Alberta, 2016), as shown in Figure 1. The oil sands sector is the second largest source of SO₂ and
179 the third largest source of industrial NO_x in the province of Alberta. This sector is also a significant source of
180 industrial PM, CO, and Volatile Organic Compound (VOC) emissions (Zhang *et al.*, 2018), from a variety of source
181 types and industrial processes (*e.g.* open pit mine tailings ponds, large diesel fleets, bitumen upgrading facilities).
182 As is described below, very high resolution emissions data are available for these sources, and emissions take place
183 in a region with significant topography, hence the region provides a good test case for the relative impact of grid
184 cell size on air-quality model prediction results.

185 We describe next our model, the simulation domains and forecasting setup, the emissions data, our evaluation
186 methodology, and the results of our analysis.



187

188 Figure 1. Map showing the Oil Sands regions (Government of Alberta, 2016).

189 2. Methodology

190 191 1.1 GEM-MACH

192 The air-quality model used in this work is Environment and Climate Change Canada's (ECCC) Global Environmental
193 Multiscale – Modelling Air-quality and Chemistry (GEM-MACH) model, which has been in use as Canada's
194 operational air-quality forecast model since 2009 (Moran *et al.*, 2010). GEM-MACH is an on-line model, that is,
195 both meteorological and chemistry processes are handled within a single model. The chemical processes reside
196 within the physics module of the Global Environmental Multiscale meteorological forecast model (Côté, *et al.*,
197 1998(a,b)), originate with Environment Canada's earlier off-line model (A Unified Regional Air-quality Modelling
198 System; AURAMS, Gong *et al.*, 2006), and include process representation for particle microphysics (Gong *et al.*,
199 2003(a,b)), inorganic heterogeneous chemistry (Makar *et al.*, 2003), aqueous phase chemistry, in-cloud and below-
200 cloud scavenging (Gong *et al.*, 2006), and secondary organic aerosol formation (Stroud *et al.*, 2011). GEM-MACH
201 employs a sectional approach to represent the size distribution of atmospheric particles, with 12-bin (Makar *et al.*,
202 2015(a,b); Gong *et al.*, 2015) or 2-bin configurations (Moran *et al.*, 2010). The latter configuration is designed for
203 maximum computational efficiency, with re-binning to the 12-bin distribution for key particle microphysics
204 processes, in order to improve accuracy. Here, the 2-bin version of the model has been used, the main focus of the
205 work being the impact of horizontal grid cell size on model results. Eight aerosol chemical components are resolved
206 in GEM-MACH (sulphate, nitrate, ammonium, elemental carbon, primary organic aerosol, secondary organic
207 aerosol, sea-salt and crustal material). In the present study, we make use of GEM-MACH v.1.5.1, described in more
208 detail in Makar *et al.*, 2015(a,b), employing 80 levels in a hybrid vertical coordinate system extending up to 0.1hPa
209 (~30km). Both model grid cell size simulations compared here (2.5km and 1km grid cell sizes, see below) make use
210 of the Milbrandt-Yau double moment explicit microphysics scheme, that is, cloud processes are resolved explicitly
211 at these scales (Milbrandt and Yau, 2005(a,b)).

212 1.2 Model Setup

213 214 1.2.1 Grid Nesting

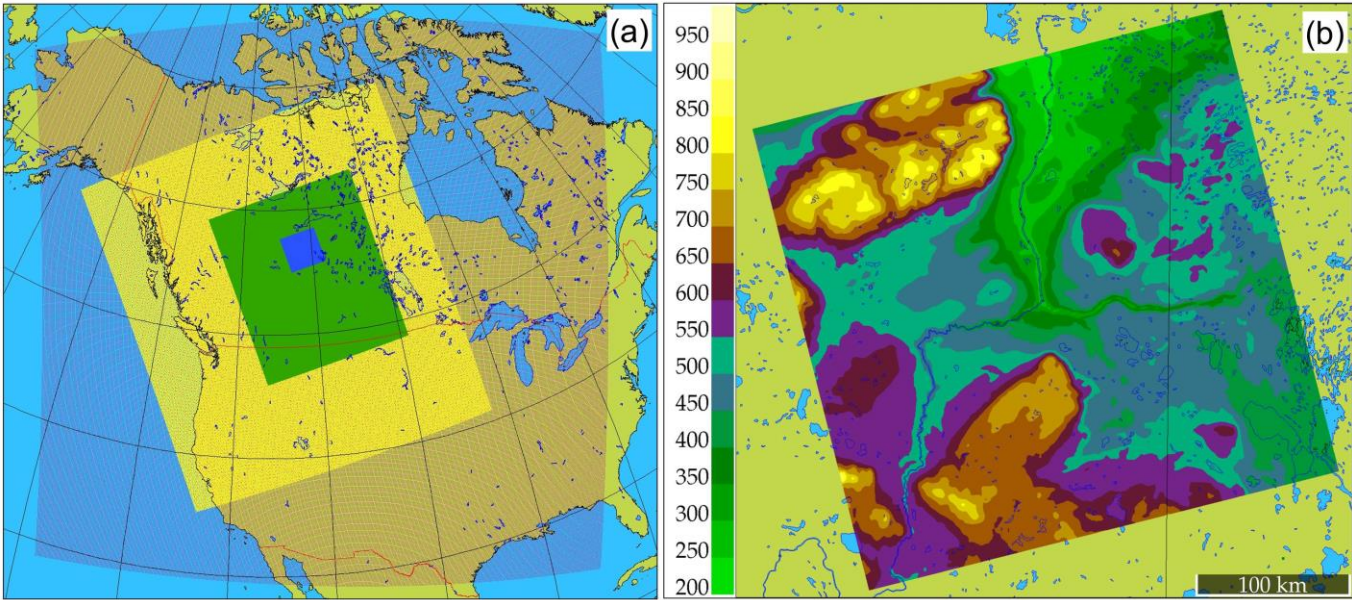
215 Four levels of nesting have been employed in our simulations, shown in Figure 2(a). This version of GEM-MACH
216 operates on a rotated latitude-longitude coordinate system wherein the position of the coordinate system poles is
217 set by the user, allowing rotations of the grid with decreasing grid cell size during nesting. The outermost nested
218 grid corresponds to the westernmost two-thirds of the operational GEM-MACH forecasting domain, with a 10km
219 grid cell size, and employ a combination of the Kain-Fritsch sub-gridscale convective cloud scheme (Kain and
220 Fritsch, 1990; Kain, 2004) and a Sundqvist (1988) for cloud parameterizations. Within that outer grid is nested a 10
221 km grid cell size western Canada domain (yellow region, Figure 2(a)) which has been rotated to match the
222 horizontal orientation of the Rocky Mountains, and which makes use of a double-moment microphysics scheme
223 (Milbrandt and Yau, 2005a,b) in place of the Sundqvist (1988) parameterization. The intention of this

224 intermediate local 10km simulation domain was to provide initial hydrometeors for the two innermost domains,
225 to reduce the “spin-up” time required for the inner domains’ meteorology to reach an equilibrium with respect to
226 cloud formation. The latter two domains (2.5km and 1km grid cell sizes) resolve the cloud microphysics explicitly
227 using the double moment scheme alone and no convective parameterization (Milbrandt and Yau, 2005a,b). The
228 third nested grid inwards (green region, Figure 2(a)) is the 2.5km grid cell size domain, which covers most of the
229 Canadian provinces of Alberta and Saskatchewan. This grid will hereafter be referred to as the OS2.5km domain.
230 The fourth and final nested grid (blue square, Figure 2(a)) is a 1km grid cell size domain, roughly centered over and
231 covering the immediate environs of the Athabasca Oil Sands, and is referred to hereafter as the OS1km model.
232 This last nest also shows the region within which 22 instrumented aircraft flights were conducted during August
233 and September of 2013, providing a unique measurement dataset for our evaluation of the OS2.5km and OS1km
234 model output for the same time period. Table 1 provides details on the horizontal dimensions of each of these
235 nested domains, and the duration of the simulations on each grid. All four model nests make use of the same
236 vertical coordinate and levels. Figure 2(b) shows the topography of the 1km domain in detail; the region to be
237 modelled is situated in a broad river valley, with a local vertical relief of 750 m. Significant wind shears and
238 frequent inversions are observed in the region, and part of our interest in 1km grid cell size simulations is to
239 determine the extent to which these local features may influence model prediction accuracy.

240 2.2.2 Simulation Cycling Strategy

241 Model simulations mimic an operational forecasting system, starting from the use of archived, data-assimilated
242 meteorological analyses as meteorological input and boundary conditions every 36 hours. The use of analysis
243 fields is a standard meteorological forecasting practice to prevent the chaotic drift of the model results from
244 observed meteorology over time. The outermost 10km domain uses initial and boundary conditions from the
245 output of a meteorological simulation, that is itself driven by an analysis field. The outermost domain model then
246 carries out a 36-hour forecast, of which the first 6 hours are discarded as spin-up; the final 30 hours are used as
247 initial and boundary conditions for the rotated 10 km grid cell size domain (the OS10km domain). An OS10km
248 simulation of 30 hours is then carried out, with the first 6 hours being discarded as spin-up, and the latter 24 hours
249 forming the initial and boundary conditions for the 2.5 km grid cell size OS2.5km simulation. The OS2.5km
250 simulation is of 24 hours duration. The OS1km simulation covers the same 24 hours (and hence both 2.5km and
251 1km simulations start from the same OS10km initial conditions at for every 24 hour forecast), with the 2.5km
252 simulation providing boundary conditions thereafter to the OS1km model. Continuity between 24 hour forecasts
253 is thus maintained at the level of the outermost nest. The outermost domain is cycled every 12 hours starting at
254 00UT and 12UT; however, we have selected the set of contiguous OS2.5km and OS1km 24 hour simulations starting
255 from the 12UT continental domain for our comparison.

256 Meteorological boundary conditions for lowest resolution GEM-MACH simulations are taken from operational



258
 259 Figure 2. (a) The four nested domains of the GEM-MACH simulations. From outermost to innermost domains,
 260 these are CONT10km (outermost, red dots), OS10km (yellow), OS2.5km (green), and OS1km (blue). The model
 261 simulations from the two innermost domains are the focus of the present study. (b) Topography in the OS1km
 262 domain centred on Fort McMurray, Alberta (m agl). The coloured area corresponds to the central blue domain in
 263 (a).

264 Table 1. Nested Domain Specifications

Parameter	CONT10km	OS10km	OS2.5km	OS1km
Grid Size	520x520	318x280	643x544	318x324
Time step size (s)	300	300	60	20
Hours simulated	36	30	24*	24*

265 *Note that both OS2.5km and OS1km output frequency was hourly.

266 2.3 Model Emissions

267 All emissions data used in this work are described in Zhang *et al.* (2018). These emissions data include (a) direct
 268 observations of stack-specific hourly emissions measured by Continuous Emission Monitoring Systems (CEMS), (b)
 269 regional emissions inventory data from the Cumulative Environmental Management Association (CEMA) - which
 270 had the most detailed stack and process level emission data for the AOSR facilities, including emissions from mine
 271 faces, tailings ponds, and the off-road mining fleet), (c) the 2010 Canadian Air Pollutant Emissions Inventory (APEI)

272 - which is the most comprehensive national emissions inventory, and which has the largest spatial coverage for
273 area sources outside the AOSR, and (d) the 2013 National Pollutant Release Inventory (NPRI) (a subset of the APEI)
274 that is based on emissions reports from large industrial facilities.

275 These emissions data sets primarily describe emissions of pollutants known as criteria-air-contaminants (NO_x,
276 VOCs, SO₂, NH₃, CO, PM_{2.5}, and PM₁₀) for *major-point sources* (*i.e.*, large emission stacks) and *area sources*. Area
277 emissions sources typically consist of multiple small mobile sources spread over a large area (*e.g.*, off-road
278 vehicles), large flux sources such as mine tailings settling ponds or mine faces, and/or large numbers of small
279 stacks for which no stack characteristic data (volume flow rates, temperatures of emissions, stack diameters),
280 needed to estimate plume-rise heights, are available.

281 Major-point sources are represented by a single geographical (latitude, longitude) pair of coordinates, and are
282 assigned to the grid cell in which the point is located. These sources are likely to be the most impacted by model
283 horizontal grid cell size, as even a large major-point source plume, which in reality may only occupy an emissions
284 horizontal area on the order of 100 m², is represented by a flux spread over an entire grid cell. A plume from a
285 major point source within a 2.5km grid cell will thus be immediately diluted to a size of 6.25km² upon emission,
286 whereas the same source with a 1km grid cell will have a cross-sectional horizontal extent of 1km². At the same
287 time, higher resolution may require a much more accurate representation of model winds close to the sources to
288 maintain accuracy in evaluation metrics dependant on plume position such as correlation – a wider plume being
289 more likely to at least partially intersect a monitoring station location than a narrower plume.

290 Area sources that are large compared to both model grid cell sizes (2.5km and 1km) can be expected to be
291 approximated by model grid cells of both resolutions, and are thus expected to be less impacted by model
292 resolution than emissions from point sources. However, smaller area sources (*i.e.* areas intermediate between
293 2.5km and 1km to the side) may be better resolved, and hence have less dilution and higher downwind
294 concentrations, when higher spatial resolution is employed.

295 In the AOSR, approximately 95% of the SO₂ emissions originate in major-point sources, while NO₂ is
296 apportioned ~40% to major-point sources and ~60% to area sources (Zhang *et al.*, 2018). Consequently our *a*
297 *priori* expectation is that the impact of the resolution change will be strongest for species like SO₂, and less strong
298 for species like NO₂ that are emitted in part by point sources, but may also be apparent for other species and
299 secondary products, such as O₃.

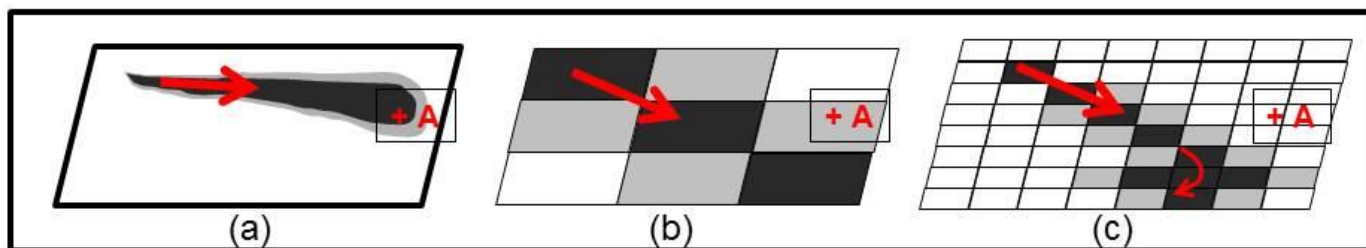
300 1.4 Model Evaluation Methodology and Metrics

301 Comparisons between air-quality models and observations usually take the approach of comparing observation
302 and model-generated values paired in time and space, from the observation location and corresponding model
303 grid-cell respectively. We refer to this approach hereafter as our “standard” evaluation, for both 2.5km and 1km

304 simulations. However, we note additional factors aside from grid-cell size may influence the outcome of air-
305 quality model evaluations. For example, the relative skill of the meteorological component of the air-quality
306 model will depend in part on the density of meteorological observation data, incorporated into the model via data
307 assimilation, for the construction of the model's initial meteorological state. This in turn will influence the local
308 skill of the model's predicted wind directions and hence the skill of its plume transport. The simulations carried
309 out here focus on the Fort McMurray area, where the nearest available upper air meteorological sounding site is
310 located at the ECCC Stony Plain station, located approximately 500km south-west of the study area. The
311 advantage of higher resolution simulations (*e.g.*, reduced numerical error associated with the discretization of
312 transport operators, and better treatment of local topographic influences) may thus be offset by errors in the
313 predicted *large scale* flow.

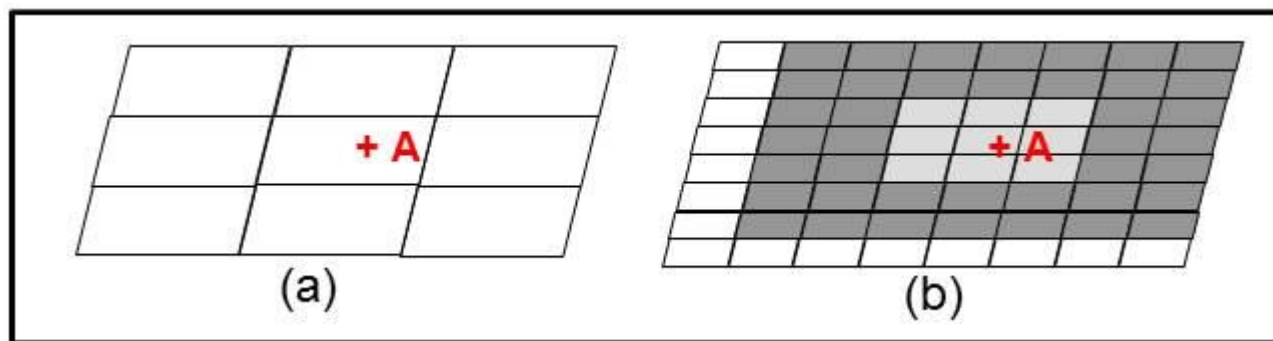
314 While meteorological model synoptic-scale forecast errors may manifest themselves locally as errors in the
315 direction of winds driving local plume transport, other advantages may result from the use of higher resolution
316 air-quality models. Since lower resolution models *de facto* instantaneously redistribute plumes emitted from
317 large stack sources over a larger area, such artificial diffusion will reduce the model's ability to accurately simulate
318 concentration maxima, and the resulting chemistry, within simulated model plumes. However, the spatial extent
319 of a plume in a model employing a large horizontal grid cell size may be such that its existence may be captured at
320 discrete observing sites. In contrast, forecast plumes in models with smaller horizontal grid cell sizes may
321 correctly capture plume magnitude and chemical behaviour, but may be more subject to errors in the larger scale
322 wind direction. To illustrate this point, Figure 3 shows a conceptual diagram of an actual plume, a large grid cell
323 size model plume, and a small grid cell size model plume, where the latter two simulated plumes are both subject
324 to the same synoptic-scale error in wind forecast direction (indicated by large red arrows; the smaller red arrow in
325 Figure 3(c) indicates the impact of local forcing predicted for the second model). Observation station "+A" is
326 located downwind, and records the presence of the actual plume (Figure 3(a)). The coarse grid cell size simulated
327 plume (Figure 3(b)), despite the error in the forecast wind direction, captures part of the observed plume in the
328 resulting time series at the observation station location. In contrast, the small grid cell size plume (Figure 3(c)),
329 despite resolving the plume shape (and plume-internal chemistry) to a greater degree than the coarse grid cell size
330 simulated plume, fails to record the presence of the plume at the observation location. A simple paired
331 observation-model time series evaluation would thus suggest that the former model has superior performance to
332 the latter model in this example, despite the latter model having created a more "realistic" plume in terms of the
333 maximum concentration reached, albeit in the wrong location, due to synoptic-scale forecast wind direction error.
334 In this particular instance, the magnitude of the smaller grid cell size simulated plume is more realistic than that of
335 the coarse grid cell size plume, but this improvement will not be captured in a standard evaluation analysis. Shifts
336 in plume location across individual grid cells away from the location of an *in-situ* observation are more likely grid
337 cell size decreases. In this example, a standard analysis would impose a more stringent expectation on the smaller

338 grid cell size simulation to correctly identify plume locations.



339
340 Figure 3. Schematic comparison of surface concentration contours and model grid cell values of a transported pollutant
341 plume from a large stack (termed a "point" source). Wind direction shown by red arrows. Monitoring station location
342 marked by "+A". (a) Actual plume. (b) Coarse grid cell size air-quality model prediction. (c) Fine grid cell size air-quality model
343 prediction. Note the change in wind direction between observations (a) and simulations (b,c) associated with errors in the
344 forecast of the synoptic wind.

345 In addition to the standard analysis, we perform additional analyses that examine the model's ability to resolve
346 plumes in the *vicinity* of the observation station, in order to attempt to evaluate the potential for higher
347 resolution simulations to provide benefits which may be masked by synoptic scale forcing errors. This strategy is
348 illustrated in Figure 4.



349
350 Figure 4. Scale diagram of the same region in (a) 2.5km grid cell size simulation and (b) a 1km grid cell size simulation.
351 Region enclosed by light grey / dark grey shading in (b) represents the nearest nine / forty-nine 1km gridpoints surrounding
352 the observation location "A".

353 Figure 4(a) shows an observation station enclosing the nine nearest-neighbour model grid-cells for a 2.5km grid
354 cell size, while Figure 4(b) shows the corresponding 1 km grid cell size map, with the nine nearest-neighbour
355 model grid-cells shown in light grey, the forty-nine nearest grid cells shown in the region enclosed in dark grey.
356 Figure 4(a) encloses a region of 56.25 km^2 ($7.5 \times 7.5 \text{ km}$), while the light grey region in Figure 4(b) encloses 9 km^2 ,
357 and the darker grey region encloses 49 km^2 .

358 As noted above, in a formal mathematical sense, the smallest region resolvable by an Eulerian grid model is twice
359 the size of the model grid cell size (relating to the Nyquist frequency of the model); hence the smallest resolvable
360 feature spans two model grid cells in each direction. However, in a practical sense, a total of nine grid cells

361 centred on the observation station must be used to allow a boundary of two grid cells in any direction. Sampling
362 any or all of the 9 grid cells in Figure 4(a) may thus be said to be representative of the model's ability to simulate
363 events occurring at discrete location "+A". The closest corresponding sampling region available to the 1 km model
364 (Figure 4(b)) is shown in dark grey. The light grey region of Figure 4(b) represents the closest 1 km grid cell size
365 region that corresponds to the single 2.5 km grid cell in which the observation station is located in Figure 4(a). We
366 attempt to ascertain model performance in these approximately equivalent regions around each observation
367 station, in the analysis that follows.

368 Our approach follows two steps:

369 (1) From the 2.5km simulation, in addition to the predicted model value at the grid-cell containing the
370 observation location, we determine the model grid-cell value in the nine grid-cells surrounding the
371 observation station location which has the closest value to that observed at the station. This represents the
372 model's "best estimate" of the value at the observation station location itself, to the model's ability to resolve
373 features at 2.5km grid cell size.

374 (2) From the 1km simulation, in addition to the model value at the grid-cell location, we select the closest value to
375 the observation value from: (a) the nearest nine grid-cells to the observation station location, and (b) the
376 nearest 49 grid-cells to the observation station location. The former represents the model's "best estimate"
377 of the value at the observation station location itself, while the latter represents the 1km model's best
378 estimate in the closest equivalent region to the limiting resolution of the 2.5km model.

379 Comparing the resulting statistical measures of each of these selected values with observations, in addition to the
380 standard analysis, thus evaluates the model's best attempt to resolve features for the specified grid cell size, and
381 allows cross-comparison of model performance within nearly equivalent areas. Cross-comparing the statistical
382 values for the different regions described above shows the model's ability to resolve features such as plumes from
383 the standpoint of the region represented at the different grid cell sizes. If synoptic-scale transport direction errors
384 creates situations similar to that depicted in Figure 3(a), a standard comparison of error would be expected to
385 show little benefit to higher resolution. However, the "best model estimate" comparisons would capture the
386 ability of the higher resolution model to more accurately simulate the magnitude of the plume, if not its spatial
387 location. Each of these selection procedures will be employed in the surface concentration comparisons which
388 follow.

389 We evaluate our model simulations against observations made at surface monitoring networks in the vicinity of
390 the Athabasca oil sands, and aboard an instrumented aircraft, the National Research Council of Canada Convair.
391 For the surface monitoring data, hourly time series of model output were matched to station time series using the
392 different strategies described above. For the aircraft observations, we extract model values through temporal and

393 spatial interpolation to the aircraft's position during the flights and only perform the standard analysis, as well as
394 examining the behaviour of the two simulations along cross-sections corresponding to the flight paths.

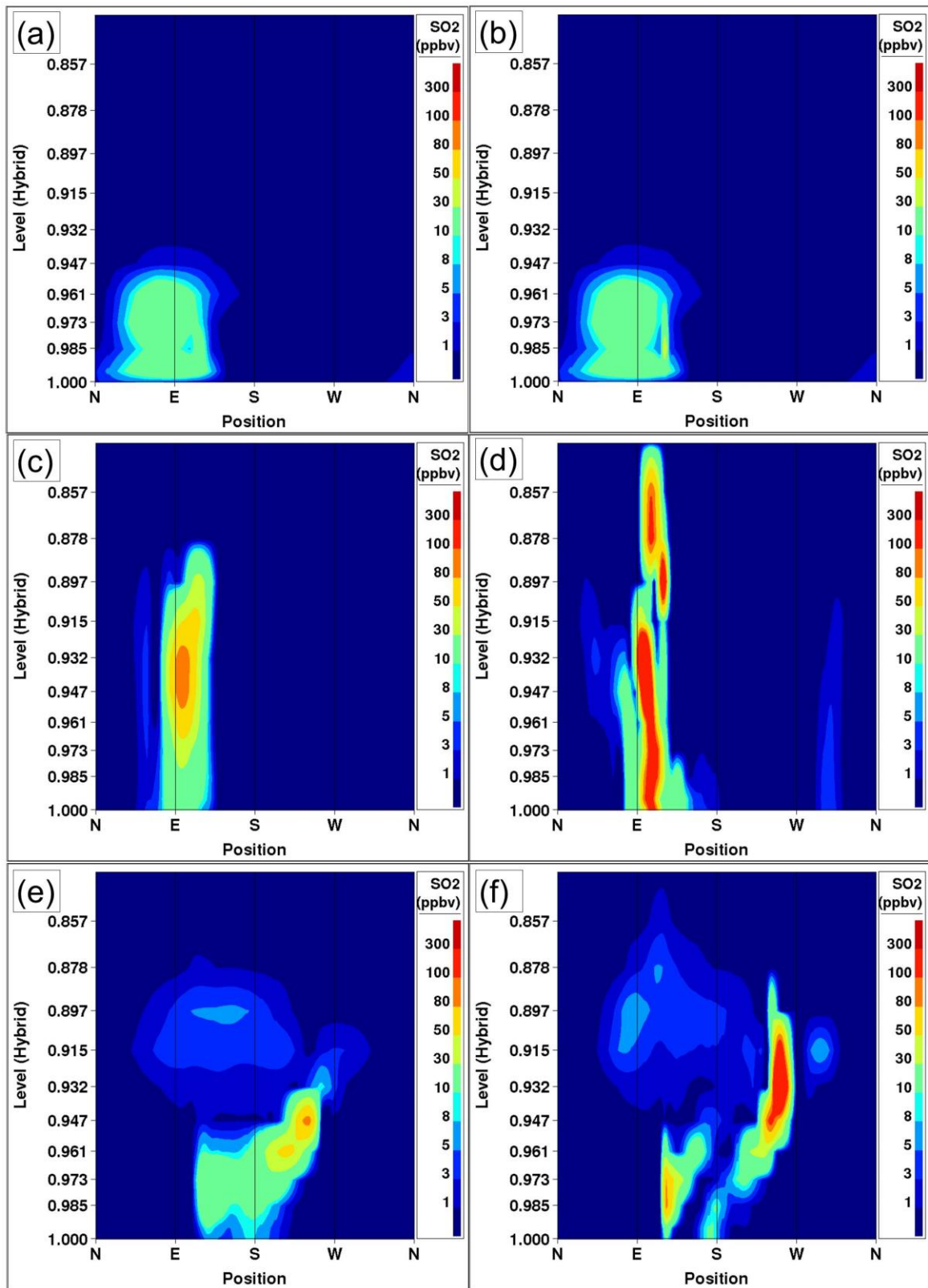
395 Our statistical metrics for evaluation are common to many other air-quality applications, and were computed
396 using the 'modstat' function from the OpenAir R package (Carslaw and Ropkins, 2012). Further discussion of
397 different metrics for model evaluation may also be found in Yu *et al.*, (2006). The statistics calculated here
398 include: mean bias (MB; perfect score: zero), mean absolute gross error (MGE; perfect score: zero), normalised
399 mean bias (NMB; perfect score: zero), normalised mean gross error (NMGE: perfect score: zero), root mean
400 squared error (RMSE; perfect score: zero), correlation coefficient (r, perfect score: unity), coefficient of
401 efficiency (COE: a perfect score is unity, a zero/negative score means the model is equivalent/less predictive
402 than the mean of the observations), and the index of agreement (IoA; perfect agreement is unity, and -1
403 indicates no agreement or little variability).

404 2 Simulation Comparisons and Evaluation

405 3.1 Model-to-model comparisons and averages

406 We begin a comparison of 2.5km and 1km grid cell size for specific events, and for averages across the 1km
407 domain, in order to provide a qualitative comparison of the differences in simulations for the two simulations, and
408 then continue with the quantitative comparison. Figure 5 compares OS2.5km (left column) and OS1km (right
409 column) simulation results for a cross-section located 0.2km from a major SO₂ emissions source at 0, 12 and 24
410 hours into a given simulation day.
411

412 The model results are identical at hour 0 due to both the OS2.5km and OS1km models being initialized from the
413 OS10km data at this time (small differences in Figure5(a,b) are due to slight mis-matches in the cross-section
414 locations). Subsequent cross-sections show the OS1km model is capable of resolving both higher absolute mixing
415 ratio values, and sharper gradients, within 12 hours of simulation time (Figure 5 (c,d)). Multiple plumes are
416 resolved by 12 hours of simulation time in the 1km grid cell size simulation, along with markedly different plume
417 heights, plume structure, and a factor of two increase in the magnitude of plume mixing ratios relative to the
418 lower grid cell size simulation, and these differences persist into the 24th simulation hour (Figure 5(e,f)). Mixing
419 ratio differences of these magnitudes are to be expected given the increase in resolution, but Figure 5 shows that
420 other important aspects of the predicted plumes have changed. The plume heights are a function of predicted
421 local stability conditions in the grid-square containing the source, and the variation shown here represents a
422 substantial change in the predicted local stability for the origin sources of these plumes, resulting from the change
423 in model horizontal grid cell size.

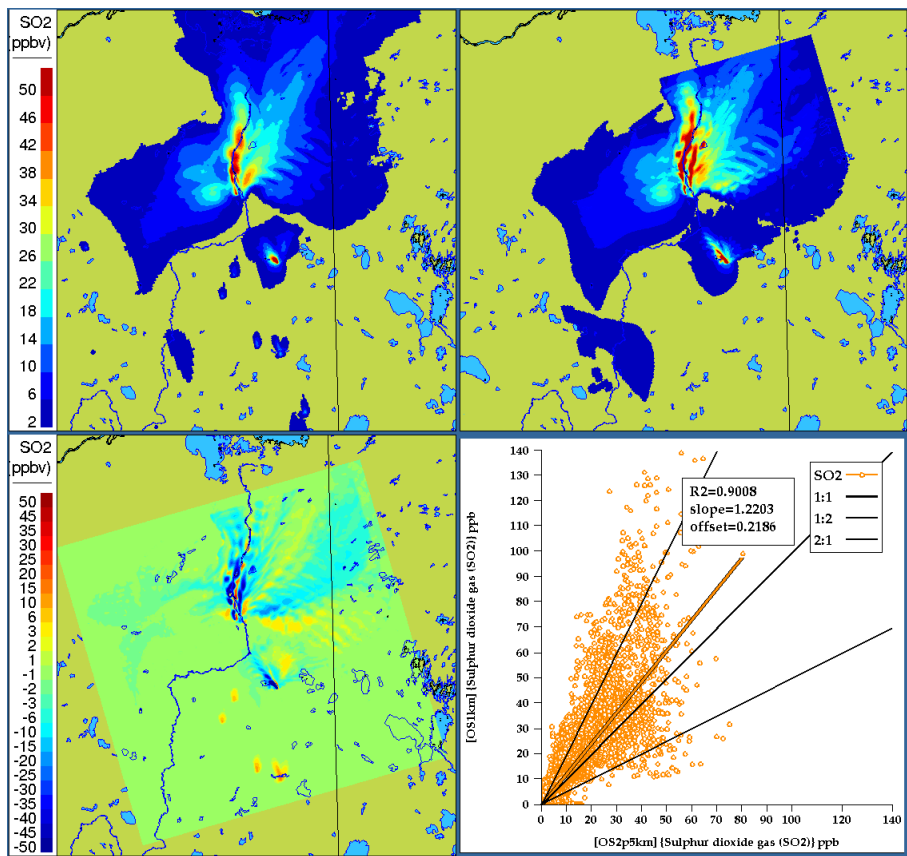


424

425 Figure 5. Comparison of simulated SO₂ plume mixing ratios (ppbv) located 0.2km from a major point source, for OS2.5km
 426 simulations (left column) and OS1km simulations (right column), at 0 (a,b), 12 (c,d), and 24 (e,f) hours into a 24 hour
 427 simulation.

428

429 Figure 6 compares the maximum surface SO₂ during the entire period for each simulation, as well as the difference
 430 in maximum SO₂ between the simulations, along with a scatterplot of OS2.5km versus OS1km simulation results.
 431 In the latter two panels, OS2.5km values were assigned to the corresponding OS1km grid-cell locations using the
 432 nearest-neighbour approach.



433
 434 Figure 6. Comparison of total-simulation *maximum* surface SO₂ mixing ratios (ppbv) at (a) 2.5km and (b) 1km grid cell size
 435 (ppbv). (c) Difference (2.5km – 1km). (d) Scatterplot of 2.5km (x-axis) versus 1km (y-axis) total simulation average grid-cell
 436 surface SO₂ mixing ratios.

437 The maximum surface concentrations tend to show more elongated structures at the smaller grid cell size,
 438 comparing Figures 6(a,b), particularly for plumes in the western (left) half of the OS1km domain. The difference
 439 plot (Figure 6(c)) shows that local maximum concentration differences of up to -45 ppbv occur, due to changes in
 440 the placement and maximum concentration of high concentration plumes. The scatterplot of Figure 6(d) shows
 441 that OS1km model has a demonstrated ability to achieve higher concentrations than the OS2.5km model, with a
 442 slope of 1.22, and a noticeable clustering of values along the 1:2 line. While these results are not unexpected
 443 since approximately 95% of the SO₂ emissions in the domain originate in large stack, or point, sources, and hence
 444 initial concentrations at source would be expected to 6.25x higher in the OS1km simulation, they also suggest that
 445 a substantial improvement in the OS1km model's ability to capture SO₂ concentrations *should* be possible. That is,
 446 the results of the two models are substantially different, and given the reduction in numerical error expected with

447 employing a smaller grid cell size, the latter might be expected to outperform a larger grid cell size model.
448 However, as we shall demonstrate in the next section, plume placement errors such as depicted in Figure 3 play a
449 substantial role in model performance as grid cell size decreases.

450 3.2 Quantitative comparisons

451 3.2.1 Surface observation comparison

452 The locations of the local network of 10 surface monitoring stations located near the sources of emissions in the
453 region (oil sands facilities) are shown in Figure 7. As noted in section 2.4, we carry out several analyses:

454 (1) The standard evaluation (model values are extracted from the model grid-cells containing the observation
455 stations, at both grid cell sizes).

456 (2) Equal areas of representativeness, 1km and 2.5km grid cell sizes (the nearest nine OS1km grid cells are
457 compared to the OS2.5km single cell evaluation in two ways):

458 a. Averaging of the OS1km results across the nine grid cells prior to evaluation (to determine whether
459 the mean value is better represented by the smaller grid cell size, similar to the approach taken in
460 Kang *et al.* (2007)).

461 b. Selection of the *best* of the nine grid cells (closest to the observation value), to determine the extent
462 to which the OS1km model is capable of better representing the concentrations somewhere within
463 the corresponding OS2.5km model grid cell, if not at the OS1km cell closest to the observation
464 location. Higher scores for the 1km grid cell size simulation in this case would indicate that while
465 errors in plume positioning (for example due to errors in the synoptic scale flow) negate some of the
466 advantages of the OS1km simulation, the plume may be better represented by the OS1km simulation
467 within the 2.5km grid cell's area.

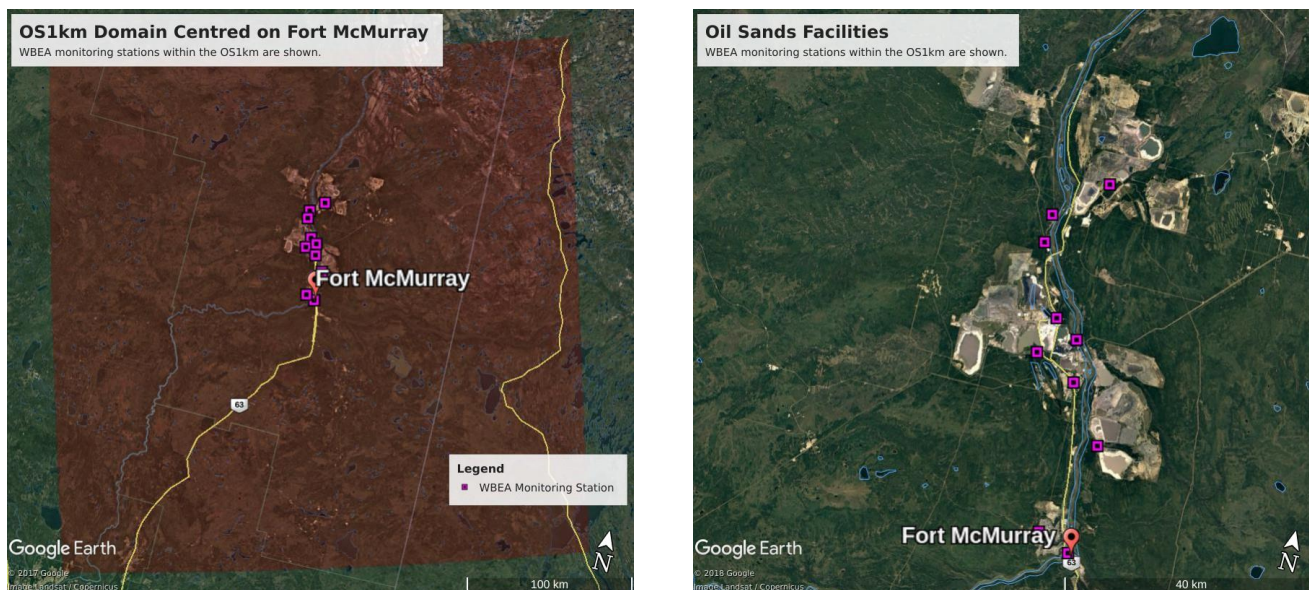
468 (3) Equal areas of representativeness and equal regions of variability (nearest nine 2.5km cells are compared to
469 the nearest forty-nine 1km cells). Here we make the assumption that the 2.5km grid cell size model's ability
470 to resolve features is limited to the surrounding three grid cells in each horizontal dimension, and make use of
471 the closest-in-size block of corresponding 1km cells (a 7×7 grid centered on the cell containing the
472 observation point). In both cases, the model value closest to the observations is chosen prior to evaluation.
473

474 While evaluations (2b) and (3) deliberately select the "best" value, they also provide a quantitative estimate of
475 the extent to which each model is capable of achieving the correct answer within roughly equal representative
476 areas centered on the observation station locations. These comparisons are intended to evaluate (a) the
477 extent to which the 1km grid cell size is capable of improving simulation results despite, *e.g.*, the larger scale
478 flow resulting in errors in the plume placement, and (b) whether the 1km grid cell size model is capable of

479 outperforming the 2.5km grid cell size model *over equivalent regions*. In the last test, we place both models on
480 an equal footing with regards to the region being represented, as well with regards to allowing cell-to-cell
481 variability and the selection of a closest match to observations.

482 Our evaluation is presented as tables of statistical metrics. The comparisons employing the nearest neighbour
483 approach are described with a “B#” superscript suffix, denoting that the “Best” sample within a square centred
484 on the observation point containing a total of # grid cells (e.g. the OS1km^{B9} label denotes a comparison
485 between observed data and the simulation grid cell within a 3 × 3 grid-cell square centered about the
486 observation point). Similarly, an A# superscript describes a comparison between the observations and the
487 Average of the # square of grid cells centered on the observation point.

488 Comparisons to surface concentrations were performed using publicly available data collected by the Wood
489 Buffalo Environmental Association (WBEA), which operates the air-quality monitoring network residing within
490 the OS1km domain. The monitoring station locations are shown in Figure 7. The statistical performance of the
491 models, calculated using the procedure outlined above, are given in Tables 2 through 5, for SO₂, NO_x, O₃, and
492 PM_{2.5}, respectively.



493
494 Figure 7. Illustration of the OS1km domain, with observation station locations. (a) Entire domain. (b) Close-up
495 view of station locations. Monitoring stations are shown as purple outline squares in both images. Light grey
496 regions in the background satellite image (b) are oil sands open-pit mining operations.

497 In the *standard* model grid cell to observation measurement comparison for SO₂, and NO_x (first two columns,
498 Tables 2 and 3), the OS1km simulation had *worse* scores for all the metrics considered here. For O₃, the OS1km
499 model had the better score for the correlation coefficient and root mean square error, and worse scores for all
500 remaining model evaluation metrics. For PM_{2.5}, the OS1km model had higher performance for the correlation

501 coefficient and biases, while the OS2.5km model outperforms the OS1km model for all other metrics examined
502 here. Based on a standard analysis, the OS1km model thus performs poorly compared to the OS2.5km model; the
503 expected advantages associated with reduced numerical error in transport at smaller grid cell sizes are being offset
504 by other factors controlling the net model error.

505 When the standard evaluation is compared to the *average* of the nearest nine 1km simulation grid cells
506 surrounding the observation point (third column of the tables), an intermediate result appears. For SO₂ (Table 2)
507 the nine-cell OS1km average has the best performance for correlation coefficient - indicating a better time
508 distribution of events may be achieved by a nine cell average at 1km grid cell size. The other metrics for the A9
509 simulation are intermediate between the two standard evaluations for each simulation, indicating that some of the
510 performance loss resulting from the use of 1km grid cell size is reduced through averaging results to approximately
511 the same size regions as the OS2.5km grid cell size. The latter result holds for all metrics for NO_x (including R, see
512 Table 3). For ozone (Table 4), averaging the nine nearest OS1km grid cells prior to measurement gives the best
513 performance for R and RMSE, and worse performance for the other metrics. For PM_{2.5} (Table 5), all metrics for the
514 OS1km nine grid-cell average aside from the bias fall mid-way between the two standard methodology evaluations.
515 Averaging the smaller grid cell size model results thus shows a marginal improvement, depending on the species,
516 but overall does not compensate for the decrease in performance resulting from going to the smaller grid cell size.

517 We next ask the question, “Does a more accurate simulation value *exist* within the same region of the 1km model
518 as is encompassed by a 2.5km grid cell?” (fourth column of these Tables), by selecting the model value in the
519 nearest nine 1km grid cells with the closest match to observations and comparing to the corresponding single
520 2.5km grid cell. A dramatic improvement in the relative OS1km performance metric scores can be seen. For each
521 of Tables 2 through 5, this “best of nine” 1km comparison outperforms the previous 3 comparisons (columns 1
522 through 3), for all metrics. These improvements are sometimes dramatic (*e.g.* a doubling of correlation coefficient
523 along with a reduction in mean bias by a factor of three, a reduction of NO_x mean bias values by a factor of 3, a shift
524 of coefficient of error from negative to positive values for O₃, and a reduction in the coefficient of error for PM_{2.5} by
525 a factor of 2.5 compared to the nearest competing value from the previous evaluations. The coefficient of
526 efficiency for SO₂ and O₃ make the transition from negative to positive values when the “best-of-nine” methodology
527 is used, indicating that the model is able to better predict the observations than the observed mean, somewhere
528 within an equivalent area. This evaluation suggests that the OS1km model does *contain* a better result within the
529 same approximate region encompassed by a 2.5km grid cell. However, the location of that better result may be
530 subject to positioning error, such as described in Figure 3.

531 A valid argument could be made that the methodology employed in this fourth evaluation is subject to selection
532 bias, in that the selection of a *best* value in the case of the nearest nine 1km simulation places that model
533 simulation at an advantage relative to the 2.5km model. To address this last issue, the final two additional

534 methodologies for evaluation were employed, still maintaining the same approximate area of representativeness
535 for a grid cell, namely choosing the best value out of the nearest *nine* 2.5km grid cells (the limiting resolution of this
536 model simulation), and the best value out of the nearest *forty-nine* 1km grid cells (fifth and sixth columns of Tables
537 2 through 5, respectively). That is, we attempt to place the two models on an equal basis with regards to selection
538 bias within a given region containing an observation station.

539 Two important results can be seen from this final evaluation. First, as was the case for the “Best of 9” for the
540 OS1km simulation compared to the standard OS1km evaluation, the “Best of 9” for the OS2.5km simulation has a
541 considerably better performance than the standard OS2.5km evaluation (compare fifth and first columns, Tables 2
542 through 5). That is, the OS2.5km model may *also* be subject to location errors in transported species representation
543 which influence model performance. However, when performance within the 56.25 km² area surrounding each
544 measurement point in the OS2.5km “Best of 9” evaluation is compared to the 49 km² area surrounding the
545 measurement points in the OS1km “Best of 49” simulation (*i.e.* compare columns five and six in Tables 2 through 5),
546 it can be seen that the OS1km model outperforms the OS2.5km model for all metrics for O₃, and PM_{2.5}, and all
547 metrics aside from bias for SO₂ and NO_x. That is, despite the OS1km model having a slight disadvantage in the
548 relative size of the representative area containing the measurement station location, and both models being
549 allowed a similar selection strategy, the OS1km model is capable of generating values closer to the observations
550 than the OS2.5km model within an equivalent sub-region, across most of the metrics and chemical species
551 considered here.

552 This final result is strongly suggestive of the presence of issues such as illustrated in Figure 3. These may include
553 errors in the larger scale synoptic wind flow, combined with the reduced size of plumes as grid cell size is reduced,
554 leading to more “misses” than “hits” for a given recorded event at a measurement station compared to the coarse
555 grid cell size model. There may be multiple additional causes for such errors (examples include poor observation
556 density in the region for model initialization, underlying lower resolution boundary condition fields such as
557 topography not improving with the reduction in grid cell size, inaccuracies in land use fields used in meteorological
558 modelling due to rapid development, and errors in other aspects of the reaction transport modelling system aside
559 from horizontal resolution). The expected advantages of the small grid cell size, such as better representation of
560 the concentrations of species within plumes and hence better representation of their reactive chemistry (*c.f.*
561 Lonsdale *et al.*, 2012), may be lost in a standard performance analysis due to these other issues.

562 Our analysis suggests that a practical limit in the benefits of increasing model accuracy may be reached when
563 resolution exceeds some threshold, as a result of other errors inherent in the modelling system. However, the
564 analysis also suggests that if these non-resolution-related errors are corrected, the benefits of adopting a smaller
565 grid cell size may be substantial. For example, meteorological data assimilation employing a dense monitoring
566 network for a specific area of interest would be expected to show a greater impact for smaller than larger grid cell

567 sizes, due to the greater ability of the former to take advantage of the observation density in correcting the initial
 568 meteorological state. We note that recent work applying land use data assimilation (Carrera *et al.*, 2015) to
 569 regional 2.5km grid cell size weather simulations (Milbrandt *et al.*, 2016) have suggested that such data assimilation
 570 may indeed improve forecast skill at the very local scale.

571 Table 2. Surface SO₂ observations to model comparison for entire simulation period (ppbv)

Evaluation Metric	OS2.5km	OS1km	OS1km ^{A9}	OS1km ^{B9}	OS2.5km ^{B9}	OS1km ^{B49}
Index of Agreement	0.237	0.154	0.207	0.601	0.701	0.810
Pearson Correlation Coefficient	0.290	0.230	0.295	0.604	0.672	0.848
Normalized Mean Gross Error	2.128	2.363	2.212	1.114	0.834	0.529
Mean Gross Error	2.918	3.240	3.034	1.528	1.143	0.725
Coefficient of Error	-0.525	-0.693	-0.585	0.202	0.403	0.621
Root Mean Square Error	7.063	9.665	7.876	4.436	3.671	2.618
Normalized Mean Bias	1.130	1.376	1.299	0.347	-0.010	0.017
Mean Bias	1.550	1.887	1.781	0.475	-0.013	0.024

572 • 5466 Samples used

573 Table 3. Surface NO_x observations to model comparison for entire simulation period (ppbv)

Evaluation Metric	OS2.5km	OS1km	OS1km ^{A9}	OS1km ^{B9}	OS2.5km ^{B9}	OS1km ^{B49}
Index of Agreement	0.177	0.138	0.152	0.416	0.589	0.665
Pearson Correlation Coefficient	0.143	0.114	0.116	0.165	0.305	0.388
Normalized Mean Gross Error	1.520	1.593	1.567	1.079	0.760	0.619
Mean Gross Error	12.898	13.518	13.296	9.156	6.447	5.255
Coefficient of Error	-0.646	-0.725	-0.697	-0.168	0.177	0.329
Root Mean Square Error	28.052	35.197	34.644	25.782	15.315	13.704
Normalized Mean Bias	0.493	0.570	0.542	0.174	-0.027	-0.063

Mean Bias	4.183	4.834	4.597	1.477	-0.231	-0.531
-----------	-------	-------	-------	-------	--------	--------

574

- 3257 Samples used

575

Table 4. Surface O₃ observations to model comparison for entire simulation period (ppbv)

Evaluation Metric	OS2.5km	OS1km	OS1km ^{A9}	OS1km ^{B9}	OS2.5km ^{B9}	OS1km ^{B49}
Index of Agreement	0.414	0.405	0.404	0.527	0.637	0.690
Pearson Correlation Coefficient	0.496	0.506	0.515	0.606	0.688	0.738
Normalized Mean Gross Error	0.660	0.670	0.672	0.534	0.410	0.349
Mean Gross Error	10.757	10.915	10.949	8.692	6.673	5.687
Coefficient of Error	-0.172	-0.189	-0.193	0.053	0.273	0.380
Root Mean Square Error	16.040	15.859	15.794	13.305	11.084	9.719
Normalized Mean Bias	0.527	0.559	0.579	0.463	0.337	0.304
Mean Bias	8.579	9.104	9.431	7.536	5.488	4.945

576

- 2189 Samples used

577

Table 5. Surface PM_{2.5} observations to model comparison for entire simulation period (µg m⁻³)

Evaluation Metric	OS2.5km	OS1km	OS1km ^{A9}	OS1km ^{B9}	OS2.5km ^{B9}	OS1km ^{B49}
Index of Agreement	0.280	0.262	0.267	0.412	0.508	0.572
Pearson Correlation Coefficient	0.201	0.216	0.214	0.314	0.376	0.466
Normalized Mean Gross Error	0.791	0.811	0.806	0.647	0.541	0.471
Mean Gross Error	5.342	5.478	5.441	4.365	3.651	3.181
Coefficient of Error	-0.439	-0.476	-0.466	-0.176	0.016	0.143
Root Mean Square Error	8.286	8.786	8.663	7.117	6.169	5.690
Normalized Mean Bias	-0.268	-0.257	-0.257	-0.289	-0.299	-0.287
Mean Bias	-1.812	-1.734	-1.736	-1.948	-2.016	-1.937

578

- 3377 Samples used

579 The surface observation data were also analyzed by time-of-day, with both observations and simulations split into
 580 daytime (hours 9:00 to 18:00 local time) and nighttime (hour 19:00 to 8:00 local time) data pairs (Appendix, Tables
 581 A1 through A8, Carslaw and Ropkins, 2012). Within each of these diurnally segregated time periods, the broad
 582 aspects of the comparison were the same as for the “all data” Tables 2 to 5 above: the OS1km simulations tended
 583 to have reduced performance in a standard analysis, averaging improved but not completely ameliorated the
 584 performance of the OS1km simulation, a methodology employing the best of nine OS1km grid cells had superior
 585 performance to the two standard comparisons, and comparison of the “best of” methodologies for equal areas
 586 showed better performance for the OS1km compared to the OS2.5km simulation. We also noted substantial
 587 differences in the day and night performance of both models across the methodologies. For example, daytime SO₂
 588 and NO_x performance within a given model and comparison methodology was usually better than nighttime
 589 performance for IOA,R, NMGE, COE and NMB, while worse for RMSE, while nighttime O₃ performance was better
 590 for IOA, r, NMGE, and COE. Daytime PM_{2.5} performance was better than nighttime for IOA, r, COE, and NMB. The
 591 study area is located in a broad river valley with frequent slope-defined anabatic/akatabic and drainage flow
 592 events. These often have a diurnal nature, and may explain part of the day/night differences. Example sources of
 593 these differences may include the relative ability of the driving meteorological model to capture daytime versus
 594 nighttime mixed layer turbulence and the planetary boundary layer height.

595 3.2.2 Comparisons to Aircraft Observations

596 Twenty-two aircraft observation flights were carried out during the study simulation period – we present
 597 statistical comparisons using the standard approach only, here (model grid cell containing the observation point to
 598 observation data at the aircraft location). Model values were linearly interpolated in time and space to the
 599 aircraft observation locations and times (aircraft observations were on a 10s interval.) We begin with a composite
 600 comparison across all observation times, in Table 6.

601 Table 6. Aircraft observation comparisons, SO₂ and NO₂ (ppbv)

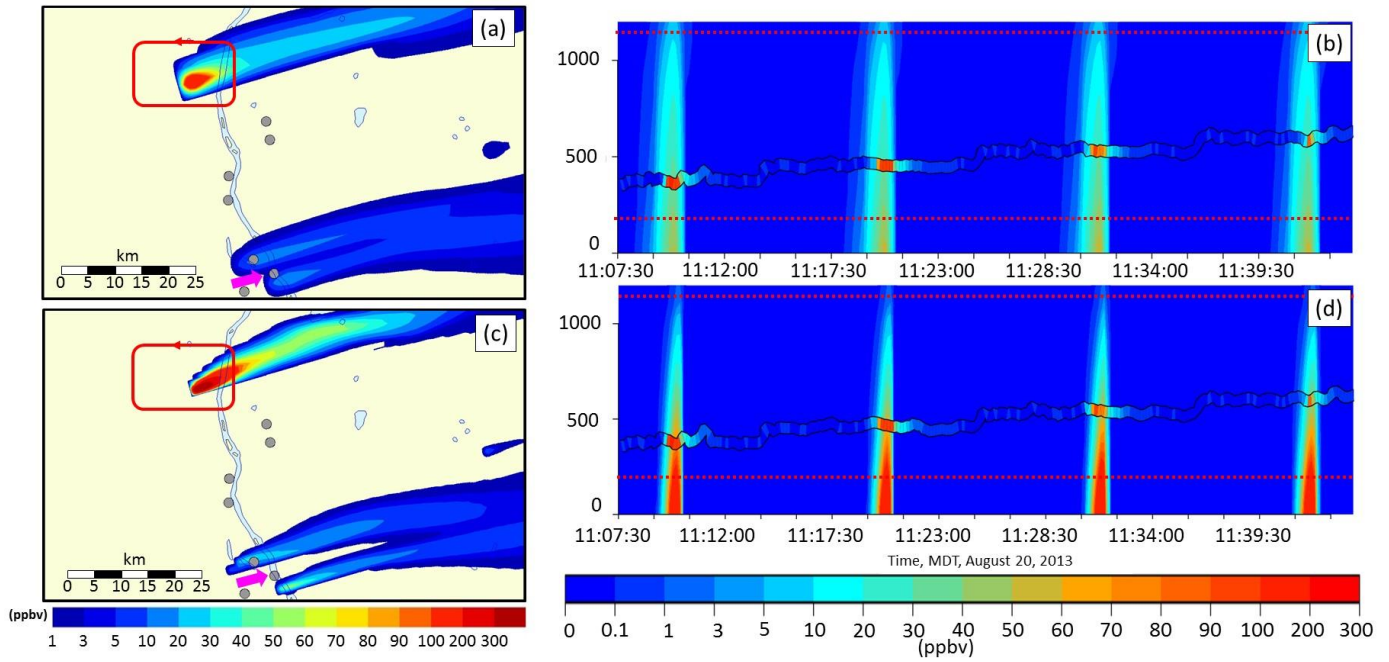
	SO ₂ (21787 samples)		NO ₂ (18310 samples)	
	OS2.5km	OS1km	OS2.5km	OS1km
Index of Agreement	0.63	0.62	0.61	0.58
Pearson Correlation Coefficient	0.26	0.28	0.39	0.34
Normalized Mean Gross Error	1.07	1.09	0.90	0.96
Mean Gross Error	3.98	4.06	1.56	1.68
Coefficient of Error	0.27	0.25	0.23	0.17
Root Mean Square Error	12.84	13.97	3.12	3.62
Normalized Mean Bias	-0.31	-0.29	-0.26	-0.20
Mean Bias	-1.17	-1.07	-0.45	-0.34

602

603 The results are in general similar to the surface analysis, in that the OS1km simulation tended to have worse
604 performance than the OS2.5km simulation (exceptions being the biases for both SO₂ and NO₂, and the slightly
605 better OS1km correlation coefficient for SO₂). One striking difference between the first two columns of Tables 2
606 and 3 and Table 14 are the magnitude of the differences between the simulations. Aloft (Table 6), the differences
607 in performance metric magnitudes between OS2.5km and OS1km simulations are much smaller than at the
608 surface (Tables 3 and 4). The biases are negative aloft, while positive at the surface, indicating that both models
609 may be lofting plumes to insufficient distances; one of the possible (non-horizontal grid cell size dependent)
610 causes of model error may be in the extent of vertical transport. This possibility is examined in more detail in
611 Akingunola *et al.* (2018, and Gordon *et al.* (2018). An example of this behaviour is shown in Figure 8; both plumes
612 fumigate to the surface, while the observed plume resides largely aloft. The OS1km model captures the higher
613 concentrations to a better degree, but the impact of excessive fumigation more than offsets this improvement, as
614 is shown by the performance evaluation of Table 7, where both models have negative biases aloft. In this
615 particular case, the tendency of the model to overestimate the extent of fumigation has a bigger impact on
616 performance than grid cell size. Garcia-Menendez *et al.* (2014) have noted similar results for forest fire plume
617 prediction.

618 Panels (a) and (c) of Figure 8 provide a further example of the kind of situation referenced in Figure 3; surface
619 monitoring station locations are depicted as grey circles, one of which is identified with a pink arrow. This station
620 lies within the plume at 2.5km resolution (Figure 8(a)), and outside of the plume at 1km resolution (Figure 8(c)).
621 While the plume direction is the same at both scales, that is, the large-scale wind field controls the positioning of
622 the plume axis, the smaller grid cell size simulation places a stronger constraint on the accuracy of the wind field.
623 For example, if the simulated large-scale flow direction was inaccurately predicted by only a few degrees, the
624 plume would not appear in the 1km simulation time series at this location, while registering as present in the
625 2.5km simulation. Nevertheless, the plume maximum concentration is better captured by the smaller grid cell size
626 simulation (compare maximum values in observed aircraft SO₂, Figure 8 (b, d)). The higher resolution simulation
627 may thus more accurately simulate the plume maximum concentration – but not its placement in space, as was
628 hypothesized in Figure 3.

629



630

631 Figure 8. Comparison between OS2.5km (a,b) and OS1km (c,d) simulations for SO₂ relative to aircraft observations
 632 (ppbv). (a,c): Simulated surface concentrations of SO₂, with the flight track shown as a red line. Grey circles:
 633 surface monitoring station locations; pink arrow indicates a station located inside a plume at 2.5km resolution (a),
 634 and outside the plume at 1km resolution (c). (b,d): Portion of the simulated concentration profiles along the flight
 635 path as a function of time. Successive intersections of the flight path with the plume appear as background colour
 636 contours; observed SO₂ aboard the aircraft is shown between the two black lines. Vertical axis is elevation above
 637 the ground; the aircraft elevation is increasing with successive passes around the facility. Dotted lines show the
 638 upper and lower vertical extent of the observed plume; note that for both model simulations, the plume
 639 erroneously fumigates the surface.

640

641 Table 7. Standard performance evaluation of Flight 8 for SO₂ (ppbv)

	OS2.5km	OS1km
Index of Agreement	0.69	0.68
Pearson Correlation Coefficient	0.42	0.31
Normalized Mean Gross Error	1.04	1.09
Mean Gross Error	4.02	4.25
Coefficient of Error	0.39	0.35
Root Mean Square Error	16.72	20.57
Normalized Mean Bias	-0.42	-0.34
Mean Bias	-1.63	-1.32

642 1261 samples used.

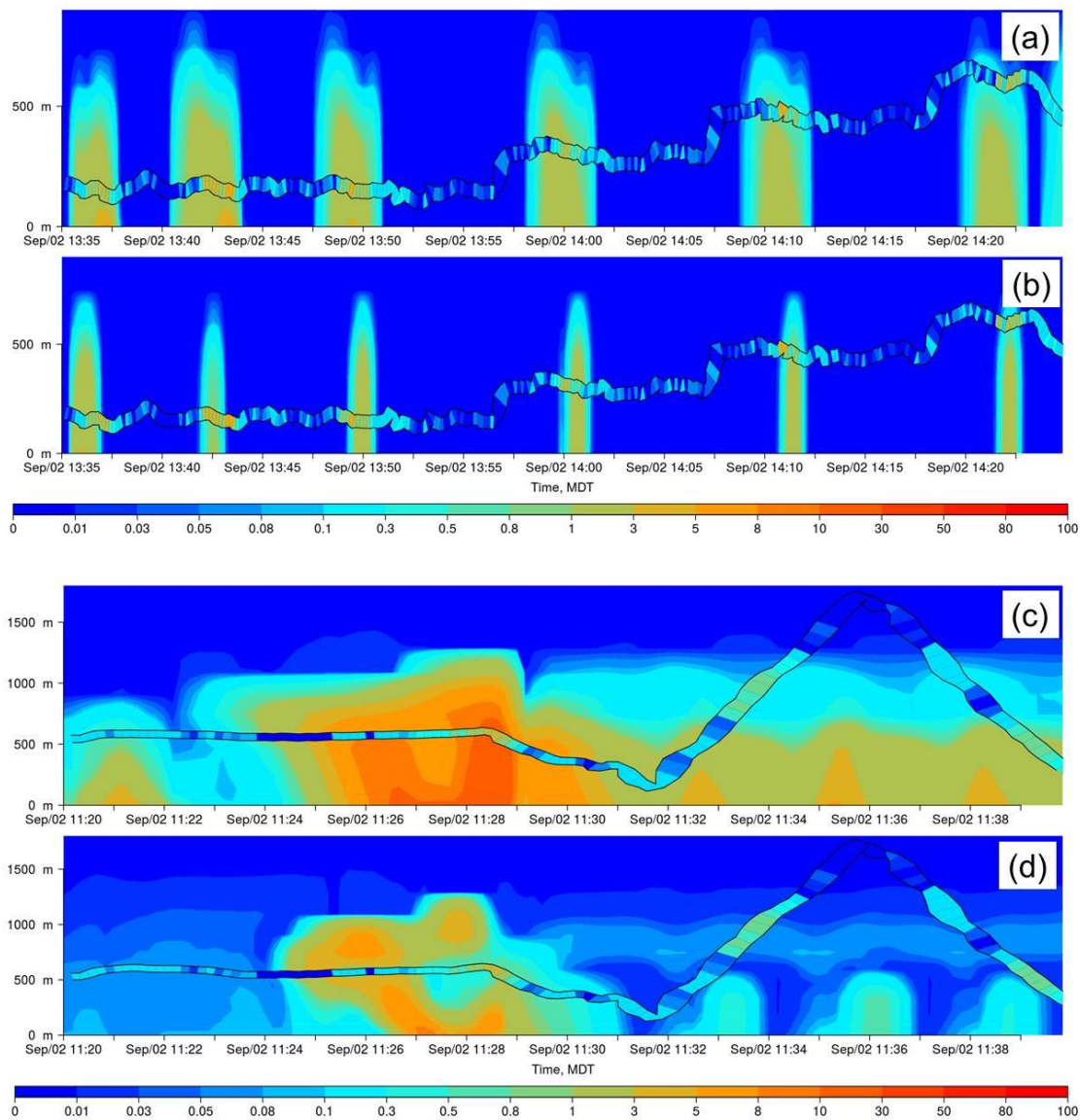
643 Meanwhile other flights show a clear advantage of the OS1km model. One example is given by the NO₂
 644 performance evaluation of Table 8 and depicted in Figure 9, for Flight 17 (a similar flight plan carried out around
 645 the same facility as Flight 8). While the correlation coefficient degraded slightly in the OS1km resolution
 646 simulation, all other performance measures were improved with the decrease in grid cell size. Two time versus
 647 height profile cross-sections for Flight 17 are shown in Figure 9. In the upper two panels, the OS2.5km (Figure
 648 9(a)) and OS1km (Figure 9(b)) simulations are compared for the portion of the overall flight track circling the given
 649 facility. This comparison clearly shows that the OS1km model does a better job of capturing the width of the high
 650 concentration region of the plume – however, the location of the model plume lags the observations. During this
 651 portion of the flight alone, the OS2.5km model statistics, particularly the correlation coefficient, outperform the
 652 OS1km model, due to this issue of plume location mismatching. Figures 9(a,b) may be compared to Figure 3(a,b) –
 653 the same situation is depicted in both Figures. Figure 9(c,d) show the OS2.5km simulation (10(c)) and OS1km
 654 simulation results in another portion of the flight – here the OS1km performance for most statistics was better
 655 than the OS2.5km model performance. The OS1km model (Figure 9(d)) captures the existence of a lower
 656 concentration layer aloft in the right-hand side of the cross-section, and the existence of low concentration
 657 intervening layers, as well as the overall lower concentrations of SO₂, while the OS2.5km model does not resolve
 658 these fine scale and lower concentration features. We note here that IoA, CoE and the other error measures
 659 capture the visual impression that the OS1km model outperforms the OS2.5km model for this flight, while the
 660 correlation coefficient is highly dependent on the placement of the plume maximum in the upper two panels.

661 These and the snap-shot comparisons described in Section 3.1 show that the higher resolution model is having a
 662 significant impact on predictions – however, other aspects of the overall model performance are preventing the
 663 potential benefits of higher resolution from influencing the standard performance evaluation.

664
 665

Table 8. Standard performance evaluation of Flight 17 for NO₂ (ppbv)

	OS2.5km	OS1km
Index of Agreement	0.26	0.58
Pearson Correlation Coefficient	0.26	0.25
Normalized Mean Gross Error	2.03	1.15
Mean Gross Error	0.52	0.29
Coefficient of Error	-0.48	0.16
Root Mean Square Error	1.37	0.70
Normalized Mean Bias	0.83	-0.54
Mean Bias	0.21	-0.14



668 Figure 9. Flight 17 comparison for NO₂ (ppbv) for portions of the net flight track circling the CNRL facility for
669 OS2.5km (a) and OS1km (b) simulations, and for a later section of the same flight path for the OS2.5km (c) and
670 OS1km (d) simulations.

4. Discussion

A key result of our current work is that 1km grid cell size simulations resulted in improved prediction of plume concentration maxima relative to 2.5km grid cell size simulations, despite having no improvement using standard scoring methodologies. We also have described a scoring approach wherein these potential advantages of higher resolution may be quantified. We believe that flow field effects such as described in Figure 3 are a general result of increasing grid resolution, but note important caveats, which include:

- (1) The availability of meteorological observation and high resolution emissions data to provide model driving information, and the resolution and proximity of this information to the simulation location. Both will influence the relative importance of grid cell size on model results. If this information is available in a higher resolution than the lower of two grid cell size simulations being compared, and/or is used via data assimilation to improve model initial meteorological conditions, our expectation is that the smaller grid cell size model may outscore the larger grid cell size model, even for more standard metrics.
- (2) The extent to which local, versus synoptic, weather conditions drive flow in a given region. For example, in the urban heat island meteorological simulations of Leroyer *et al.* (2014), the accuracy of local flow predictions was shown to be extremely dependent on the representation of the urban heat island, and the accuracy of the latter was critically dependent on the grid cell size (which in this example went down to 250 m). In this respect, for meteorological conditions wherein local factors can dominate the flow, and where those conditions may be adequately modelled only at very high resolution, we would again expect the smaller grid cell size simulation to provide better performance, for standard metrics.
- (3) Conversely, model performance using standard metrics should not be expected to *increase* with successively larger and larger grid sizes; the accuracy of even the synoptic flow field will not be captured as model resolution decreases.

Given these considerations, we recommend that modellers should attempt successively smaller grid cell sizes to determine the following: first, the point at which, for their particular system and simulation location, subsequent grid cell size reductions fail to improve performance; and second, to make use of still higher resolutions for studies wherein the point-to-point comparison is less important, and other factors such as accurately capturing the plume chemistry are more crucial.

5. Summary and Conclusions

Our work suggests the following:

Decreasing air-quality model horizontal grid cell size will not necessarily result in improvements to model performance in standard performance evaluations, in which the model values at the grid-cells encompassing measurement location stations are used in a pairwise comparison to observations. Other considerations, such as

706 the accuracy of the larger scale wind direction and speed forecast, and the accuracy of the plume rise
707 parameterization used within the model may play a greater role in the overall performance of the model, and
708 reduce the benefits of the smaller grid cell size. In the context of a standard model performance evaluation, there
709 may be fixed limits to the benefits of decreasing model grid cell size.

710 Despite this difficulty, our results also show that the use of smaller grid cell sizes have some potential benefits, in
711 that these models do a better job of resolving specific air pollution features, like high concentration maxima
712 within plumes. Both coarse and fine grid cell size plumes may be misplaced in both time and space, with the net
713 result that the latter model has a worse performance in a standard comparison, but is nevertheless more likely to
714 capture the correct in-plume concentrations, and hence the chemistry, of the actual plume, in the *neighbourhood*
715 of the observation location. When the evaluation is broadened to find the closest fit to observations in the vicinity
716 of the observation station, with models confined to a similar representative area around the observation station,
717 these potential benefits of the smaller grid cell size become apparent.

718 Our results should not be taken as an indication that the standard metrics for model comparison are in some way
719 flawed – they provide the most rigorous method for evaluating the performance of a model at specific monitoring
720 locations and specific times. However, the ancillary performance assessment methodology presented here shows
721 that models with very small grid sizes, which may have standard performance metric scores that have not
722 improved or even have degraded relative to larger grid cell size models, nevertheless have scientific value, in
723 terms of being better able to capture plume concentrations and hence plume chemistry, if not plume position.
724 The work also suggests that the prediction accuracy of very local transport conditions may be a large factor in
725 preventing the smaller grid cell size models from achieving improved performance in standard performance
726 analyses.

727 These findings suggest that at the current state of development, VHR air-quality models are of benefit for the
728 specific purpose of chemical process studies, in which the main aim of the work is to accurately simulate plume
729 chemistry – and in which accurate forecasting of the *position* of the plume in time and space is a secondary
730 concern. Our work also suggests that efforts to improve other aspects of the overall modelling framework which
731 improve the large-scale flow (for example, the use of data assimilation of local meteorology to improve wind
732 direction predictions) may result in greater benefits as smaller grid cell sizes are employed.

733

734 *Author contribution:* M.R.: computer simulations and analysis, graphical outputs, initial manuscript draft; A.H.: supervision of
735 M.R., research advice and infrastructure, manuscript writing, comments on manuscript drafts. P.A.M.: co-supervision of M.R.,
736 research advice and infrastructure, manuscript writing, lead for revisions and responses to referees. A.A.: model code
737 assistance and setup, provision of model – observation comparison and scoring package. J.Z.: provision of 2.5km and 1km
738 resolution emissions files. M.D.: provision of 2.5km and 1km resolution emissions files, comments on manuscript drafts. Q.Z.:

739 provision of 2.5km and 1km resolution emissions files.

740 *Acknowledgements.* The authors wish to thank the support of Environment and Climate Change Canada
741 (ECCC), under the CCAP program, for supporting this research. The authors also gratefully acknowledge the
742 assistance of Michel Valin and Sylvie Gravel for advice and assistance with the installation of GEM-MACH on the
743 Carleton University workstations during the early stages of this project.

6. References

- Akingunola, A., Makar, P.A., Zhang, J., Darlington, A., Li, S.-M., Gordon, M., Moran, M.D., Zheng, Q., A chemical transport model study of plume rise and particle size distribution for the Athabasca oil sands, *Atmos. Chem. Phys.*, 18, 8667-8688, 2018.
- Arunachalam, S., Holland, A., Do, B. & Abraczkas, M., A quantitative assessment of the influence of grid resolution on predictions of future-year air quality in North Carolina, USA. *Atm. Env.*, 40, 5010-5026, 2006.
- Carhart, R.A., Policastro, A.J., Wastag, M., and Coke, L., Evaluation of eight short-term long-range transport models using field data, *Atm. Env.* 23, 85-105, 1989.
- Carrera, M.L., Belair, S., Bilodeau, B., The Canadian Land Data Assimilation System (CALDAS): Description and Synthetic Evaluation Study, *J. Hydromet.*, 16, 1293-1314, 2015.
- Carslaw, D. C. and Ropkins, K., openair – an R package for air quality data analysis, *Environ. Modell. Softw.*, 27–28, 52–61, 2012.
- Ching, J., Herwehe, J. and Swall, J., On joint deterministic grid modeling and sub-grid variability conceptual framework for model evaluation, *Atm. Env.*, 40, 4935-4945, 2006.
- Coiffier, J., Fundamentals of Numerical Weather Prediction, Cambridge University Press, 363pp., 2011.
- Côté, J., Gravel, S., Méthot, A., Patoine, A., Roch, M., Staniforth, A., The operational CMC–MRB global environmental multiscale (GEM) model. Part I: Design considerations and formulation, *Mon. Wea. Rev.*, 126, 1373-1395, 1998.
- Côté, J., Desmarais, J.-G., Gravel, S., Méthot, A., Patoine, A., Roch, M., Staniforth, A., The operational CMC–MRB global environmental multiscale (GEM) model. Part II: Results. *Mon. Wea. Rev.*, 126, 1397-1418, 1998.
- Dore, A. J., Kryza, M., Hall, J.R., Hallsworth, S., Keller, V.J.D., Vieno, M., and Sutton, M.A., The influence of model grid resolution on estimation of national scale nitrogen deposition and exceedance of critical loads. *Biogeosci.*, 9, 1597-1609, 2012.
- EPA, 1999: https://www.cmascenter.org/cmaq/science_documentation/ , last accessed September 2, 2018.
- Emery, C., Liu, Z., Russell, A.G., Talat Odman, M., Yarwood, G., and Kumar, N., Recommendations on statistics and benchmarks to assess photochemical model performance, *J. Air Waste Manage. Assoc.*, 67, 528-598, 2017.
- Fox, D.G., Judging air quality model performance - summary of the AMS Workshop on Dispersion Model Performance, Woods Hole, Mass., 8-11 September 1980, *Bull. Am. Met. Soc.*, 62, 599-609, 1981.
- Fox, D.G., Uncertainty in air quality modelling – a summary of the AMS Workshop on Quantifying and Communicating Model Uncertainty, Woods Hole, Mass., September 1982, *Bull. Am. Met. Soc.*, 65, 27-36, 1984.
- Garcia-Menendez, F., Yano, A., Hu, Y. and Odman, M. T., An adaptive grid version of CMAQ for improving the

- resolution of plumes. *Atm. Poll. Res.*, 1, 239-249, 2010.
- Garcia-Menendez, F., Hu, Y., Odman, M.T., Simulating smoke transport from wildland fires with a regional-scale air quality model : sensitivity to spatiotemporal allocation of fire emissions, *Sci. Tot. Env.*, 544-553, 2014.
- Gego, E., Hogrefe, C., Kallos, G., Voudouri, A., Irwin, J.S., Rao, S.T., Examination of model predictions at different horizontal grid resolutions. *Env. Fluid Mech.*, 5, 63-85, 2005.
- Gong, W., Dastoor, A.P., Bouchet, V.S., Gong, S.L., Makar, P.A., Moran, M.D., Pabla, B., Menard, S., Crevier, L-P., Cousineau, S., Venkatesh, S., Cloud processing of gases and aerosols in a regional air quality model (AURAMS), *Atm. Res.* 82, 248-275, 2006.
- Gong, W., Makar, P.A., Zhang, J., Milbrandt, M., Gravel, S., Hayden, K.L., MacDonald, A.M., Leaitch, W.R., Modelling aerosol-cloud-meteorology interaction: A case study with a fully coupled air quality model (GEM-MACH). *Atm. Env.*, 115, 695-715, 2015.
- Gong, S.L., Barrie, L.A., Lazare, M., Canadian Aerosol Module (CAM): a size-segregated simulation of atmospheric aerosol processes for climate and air quality models: 2. Global sea-salt aerosol and its budgets. *J. Geophys. Res.* 107, 4779. <http://dx.doi.org/10.1029/2001JD002004>, 2003a.
- Gong, S. L., Barrie, L.A., Blanchet, J.-P., von Salzen, K., Lohmann, U., Lesins, G., Spacek, L., Zhang, L.M., Girard, E., Lin, H., Leaitch, R., Leighton, H., Chylek, P., Huang, P., Canadian Aerosol Module: A size-segregated simulation of atmospheric aerosol processes for climate and air quality models 1. Module development. *J. Geophys. Res.*, 108, D1, 4007, doi:10.1029/2001JD002002, 2003b.
- Gordon, M., Makar, P.A., Staebler, R., Zhang, J., Akingunola, A., Gong, W., Li, S.-M., A comparison of plume rise algorithms to stack plume measurements in the Athabasca oil sands, *Atm. Chem. Phys. Disc.*, (<https://www.atmos-chem-phys-discuss.net/acp-2017-1093/>), 2018.
- Government of Alberta, 2016: Alberta Energy: Oil Sands, <http://www.energy.alberta.ca/oilsands/oilsands.asp>, 2016, last accessed November 11, 2017.
- Grasso, L.D., The differentiation between grid spacing and resolution and their application to numerical modelling, *Bull. Am. Met. Soc.*, 81, 579-580, 2000.
- Hanha, S.R., Air quality model evaluation and uncertainty. *J. Air Poll. Cont. Assoc.*, 33, 406-412, 1988.
- Im, U., Bianconi, R., Solazzo, E., Kioutsioukis, I., Badia, A., Balzarini, A., Baró, R., Bellasio, R., Brunner, D., Chemel, C., Curci, G., van der Gon, H.D., Flemming, J., Forkel, R., Giordano, L, Jiménez-Guerrero, P., Hirtl, M., Hodzic, A., Honzak, L, Jorba, O., Knote, C., Makar, P.A., Manders-Groot, A., Neal, L., Perez, J.L., Pirovano, G., Pouliot, G., San Jose, R., Savage, N., Schroder, W., Sokhi, R.S., Syrakov, D., Torian, A., Tuccella, P., Wang, K., Werhahn, J., Wolke, R., Zabkar, R., Zhang, Y., Zhang, J., Hogrefe, C., Galmarini, S., Evaluation of operational on-line-coupled regional air quality models over Europe and North America in the context of AQMEII phase 2. Part II: Particulate Matter, *Atm. Environ.*, 115, 421-411, 2015.

- Isakov, V., Irwin, J. S., Ching, J., Using CMAQ for exposure modeling and characterizing the subgrid variability for exposure estimates. *J. App. Met. Clim.*, 46, 1354-1371, 2007.
- Jacobson, M.Z., Fundamentals of Atmospheric Modelling, Cambridge U. Press, 656pp., 1999.
- Joe, D.K., Zhang, H., DeNero, S.P., Lee, H.-H., Chen, S.-H., McDonald, B.C., Harley, R.A., and Kleeman, M.J., Implementation of a high-resolution source-oriented WRF/Chem model at the Port of Oakland, *Atm. Env.*, 82, 351-363, 2014.
- Kang, D., Mathur, R., Schere, K., Yu, S., Eder, B., New categorical metrics for air quality model evaluation, *J. App. Met. Clim.*, 46, 549-555, 2007.
- Kain, J.S., Fritsch, J.M. A one-dimensional entraining/detraining plume model and its application in convective parameterizations. *J. Atmos. Sci.* 47, 2784-2802, 1990.
- Kain, J.S., The Kain-Fritsch convective parameterization: an update. *J. Appl. Meteorol.* 43, 170-181, 2004.
- Kheirbek, I., Haney, J., Douglas, S., Ito, K., Caputo, S., Jr., Matte, T., The public health benefits of reducing fine particulate matter through conversion to cleaner heating fuels in New York City, *Env. Sci. Tech.*, 48, 13573-13582, 2014.
- Kheirbek, I., Haney, J., Douglas, S., Ito, K., and Matte, T., The contribution of motor vehicle emissions to ambient fine particulate matter public health impacts in New York City: a health burden assessment, *Env. Health*, 15:89, doi: 10.1186/s12940-016-0172-6, 2016.
- Kumar, N., Russell, A.G., Segall, E., Steenkiste, P. Parallel and Distributed Application of an Urban-to-Regional Multiscale Model. *Comp. Chem. Eng.*, 21, 399-408, 1997.
- Lee, I.Y., Numerical simulations of cross-Appalachian transport and diffusion. *Bound. Lay. Met.*, 39, 53-66, 1987.
- Li, J., Georgescu, M., Hyde, P., Mahalov, A., and Moutaoui, M., Achieving accurate simulations of urban impacts on ozone at high resolution, *Env. Res. Lett.*, 9, 114019 (11pp), 2014.
- Leroyer, S., Belair, S., Husain, S.Z., and Mailhot, J., Subkilometer numerical weather predictions in an urban coastal area: a case study over the Vancouver Metropolitan Area, *J. App. Met. Clim.*, 53, 1433-1453, 2014.
- Lonsdale, C.R., Stevens, R.G., Brock, C.A., Makar, P.A., Knipping, E.M., and Pierce J.R., The effect of coal-fired power-plant SO₂ and NO_x control technologies on aerosol nucleation in the source plumes, *Atm. Chem. Phys.*, 12, 11519-11531, 2012.
- Makar, P. A., Bouchet, V. S. & Nenes, A., Inorganic chemistry calculations using HETV--a vectorized solver for the SO₄²⁻--NO₃⁻--NH₄⁺ system based on the ISORROPIA algorithms. *Atm. Env.*, 37, 2279-2294, 2003.
- Makar, P.A., Gong, W., Milbrandt, J., Hogrefe, C., Zhang, Y., Curci, G., Zabkar, R., Im, U., Balzarini, A., Baro, R., Bianconi, R., Cheung, P., Forkel, R., Gravel, S., Hirtl, H., Honzak, L., Hou, A., Jimenez-Guerrero, P., Langer, M., Moran, M.D., Pabla, B., Perez, J.L., Pirovano, G., San Jose, R., Tuccella, P., Werhahn, J., Zhang, J., Galmarini, S., Feedbacks between air pollution and weather, part 1: Effects on weather. *Atm. Env.*, 115, 442-469,

2015(a).

Makar, P.A., Gong, W., Hogrefe, C., Zhang, Y., Curci, G., Zabkar, R., Milbrandt, J., Im, U., Balzarini, A., Baro, R., Bianconi, R., Cheung, P., Forkel, R., Gravel, S., Hirtl, H., Honzak, L., Hou, A., Jimenez-Guerrero, P., Langer, M., Moran, M.D., Pabla, B., Perez, J.L., Pirovano, G., San Jose, R., Tuccella, P., Werhahn, J., Zhang, J., Galmarini, S., Feedbacks between air pollution and weather, part 2: Effects on chemistry. *Atm. Env.*, 115, 499-526, 2015(b).

Markakis, K., Valari, M., Perrussel, O., Sanchez, O., and Honore, C., Climate-forced air-quality modeling at the urban scale : sensitivity to model resolution, emissions and meteorology. *Atm. Chem. Phys.*, 15, 7703-7723, 2015.

Milbrandt, J. A. and Yau, M. K., A multimoment bulk microphysics parameterization, Part I: analysis of the role of the spectral shape parameter, *J. Atmos. Sci.*, 62, 3051–3064, 2005(a).

Milbrandt, J. A. and Yau, M. K., A multimoment bulk microphysics parameterization, Part II: a proposed three-moment closure and scheme, *J. Atmos. Sci.*, 62, 3065–3081, 2005(b).

Milbrandt, J.A., Belair, S., Faucher, M., Vallee, M., Carrera, M.L., and Glazer, A., The Pan-Canadian high resolution deterministic prediction system, *Weather and Forecasting*, 31, 1791-1816, 2016.

Moran, M. D. Ménard, S., Talbot, D., Huang, P., Makar, P. A., Gong, W., Landry, H., Gravel, S., Gong, S., Crevier, L.-P., Kallaur, A., Sassi, M., Particulate-matter forecasting with GEM-MACH15, a new Canadian air-quality forecast model. *Air pollution modelling and its application XX*. Springer, Dordrecht, pp. 289-292, 2010.

Pepe, N., Pirovano, G., Lonati, G., Balzarini, A., Toppetti, A., Riva, G.M., and Bedogni, M., Development and application of a high resolution hybrid modelling system for the evaluation of urban air quality. *Atm. Env.*, 141, 297-311, 2016.

Pielke, R.A. Sr., Further comments on "The differentiation between grid spacing and resolution and their application to numerical modeling", *Bull. Am. Met. Soc.*, 82, 699, 2001.

Queen, A. and Zhang, Y., Examining the sensitivity of MM5--CMAQ predictions to explicit microphysics schemes and horizontal grid resolutions, Part III—The impact of horizontal grid resolution. *Atm. Env.*, 42, 3869-3881, 2008.

Salvador, R., Calbó, J. & Millán, M. M., Horizontal grid size selection and its influence on mesoscale model simulations. *J. App. Met.*, 38, 1311-1329, 1999.

Shrestha, K. L., Kondo, A., Akikazu, K. A. G. A., Inoue, Y., High-resolution modeling and evaluation of ozone air quality of Osaka using MM5-CMAQ system. *J. Env. Sci.*, 21, 782-789, 2009.

Sillman, S., Vautard, R., Menut, L. & Kley, D., O₃-NO_x-VOC sensitivity and NO_x-VOC indicators in Paris: Results from models and Atmospheric Pollution Over the Paris Area (ESQUIF) measurements. *J. of Geophys. Res.*, 108, 8563, doi:10.1029/2002JD001561, 2003.

Stroud, C.A., P.A. Makar, M.D. Moran, W. Gong, S. Gong, J. Zhang, K. Hayden, C. Mihele, and J.R. Brook, Impact of

- model grid spacing on regional- and urban-scale air quality predictions of organic aerosol. *Atm. Chem. Phys.*, 11, 3,107-3,118, 2011.
- Sundqvist, Parameterization of condensation and associated clouds in models for weather prediction and general circulation simulation. In: Schlesinger M.E. (eds) *Physically-Based Modelling and Simulation of Climate and Climatic Change*. NATO ASI Series (Series C: Mathematical and Physical Sciences), vol 243. Springer, Dordrecht, 1988.
- Thompson, T.M., and Selin, N.E., Influence of air quality model resolution on uncertainty associated with health impacts, *Atm. Chem. Phys.*, 12, 9753-9762, 2012.
- Valari, M. and Menut, L., Does an increase in air quality models' resolution bring surface ozone concentrations closer to reality?. *J. Atm. Ocean. Tech.*, 25, 1955-1968, 2008.
- Vardoulakis, S., Fisher, B. E. A., Pericleous, K., Gonzalez-Flesca, N., Modelling air quality in street canyons: a review. *Atm. Env.*, 37, 155-182, 2003.
- Wolke, R., Schröder, W., Schrödner, R., Renner, E., Influence of grid resolution and meteorological forcing on simulated European air quality: a sensitivity study with the modeling system COSMO--MUSCAT. *Atm. Env.*, 53, 110-130, 2012.
- Zhang, J, Moran, M.D., Zheng, Q., Makar, P.A., Baratzadeh, P., Marson, G., Liu, P., Li, S.-M., Emissions preparation and analysis for multiscale air quality modeling over the Athabasca Oil Sands Region of Alberta, Canada, *Atm. Chem. Phys.*, 18, 10459–10481, 2018.

7. Appendix A: Model Evaluation Statistics

Table A1: Model Comparison Statistics

Metric and Formula	Range	Ideal Score
<p><i>Index of Agreement (IOA)</i></p> $= \begin{cases} 1 - \frac{\sum M_i - O_i }{2(O_i - \bar{O})}, \text{ when } \sum M_i - O_i \leq 2(O_i - \bar{O}) \\ \frac{2(O_i - \bar{O})}{\sum M_i - O_i } - 1, \text{ when } \sum M_i - O_i > 2(O_i - \bar{O}) \end{cases}$	[-1,1]	1
<p><i>Coefficient of Error (COE)</i> = $1 - \frac{\sum M_i - O_i }{(O_i - \bar{O})}$</p>	$[-\infty, 1]$	1
<p><i>Mean Bias (MB)</i> = $\frac{1}{N} \sum (M_i - O_i) = \bar{M} - \bar{O}$</p>		0
<p><i>Mean Gross Error (MGE)</i> = $\frac{1}{N} \sum M_i - O_i$</p>		0
<p><i>Normalized Mean Bias (NMB)</i> = $\frac{\sum (M_i - O_i)}{\sum O_i} = \left(\frac{\bar{M}}{\bar{O}} - 1 \right)$</p>		0
<p><i>Normalized Mean Gross Error (NMGE)</i> = $\frac{\sum M_i - O_i }{\sum O_i}$</p>		0
<p><i>Root Mean Square Error (RMSE)</i> = $\sqrt{\frac{1}{N} \sum (M_i - O_i)^2}$</p>		0
<p><i>Pearson Correlation Coefficient (r)</i> = $\frac{\sum (M_i - \bar{M})(O_i - \bar{O})}{\sqrt{\sum (M_i - \bar{M})^2 \sum (O_i - \bar{O})^2}}$</p>	[-1.1]	1

The limits on the summations were removed for brevity; all are from $i = 1$ to N where N is the number of observation-model pairs, M_i is the i 'th model value, O is the i 'th observation value, and \bar{M}, \bar{O} are the model and observed mean values, respectively.

7. Appendix B: Day Versus Night model performance for the different testing methodologies

Table B1. Surface SO₂ observations to model comparison, daytime (9:00-18:00) (ppbv).

	OS2.5km	OS1km	OS1km ^{A9}	OS1km ^{B9}	OS2.5km ^{B9}	OS1km ^{B49}
IoA	0.374	0.286	0.352	0.712	0.762	0.872
r	0.295	0.215	0.307	0.701	0.742	0.903
NMGE	1.739	1.982	1.798	0.799	0.660	0.356
MGE	4.201	4.788	4.343	1.931	1.595	0.860
CoE	-0.253	-0.428	-0.295	0.424	0.524	0.744
RMSE	9.317	13.388	10.275	5.171	4.652	2.996
NMB	0.730	0.990	0.871	0.054	-0.166	-0.118
MB	1.764	2.391	2.104	0.132	-0.401	-0.286

- 2119 Samples used

Table B2. Surface SO₂ observations to model comparison, nighttime (18:00-9:00) (ppbv).

	OS2.5km	OS1km	OS1km ^{A9}	OS1km ^{B9}	OS2.5km ^{B9}	OS1km ^{B49}
IoA	-0.215	-0.248	-0.233	0.231	0.473	0.609
r	0.204	0.206	0.205	0.339	0.421	0.620
NMGE	3.143	3.281	3.215	1.896	1.300	0.964
MGE	2.061	2.152	2.108	1.243	0.852	0.632
CoE	-1.549	-1.607	-1.607	-0.537	-0.054	0.218
RMSE	5.055	5.450	5.450	3.802	2.858	2.313
NMB	2.166	2.328	2.328	1.076	0.394	0.361
MB	1.421	1.527	1.527	0.706	0.258	0.230

- 3347 Samples used

Table B3. Surface NO_x observations to model comparison, daytime (9:00-18:00) (ppbv).

	OS2.5km	OS1km	OS1km ^{A9}	OS1km ^{B9}	OS2.5km ^{B9}	OS1km ^{B49}
IoA	0.485	0.440	0.465	0.639	0.712	0.789
r	0.254	0.259	0.270	0.427	0.507	0.680
NMGE	0.927	1.009	0.962	0.650	0.519	0.380
MGE	7.502	8.160	7.786	5.259	4.198	3.077
CoE	-0.030	-0.120	-0.069	0.278	0.424	0.577
RMSE	14.843	15.811	15.571	11.272	9.982	7.964
NMB	-0.205	-0.069	-0.135	-0.258	-0.258	-0.216
MB	-1.659	-0.559	-1.091	-2.089	-2.091	-1.744

- 1252 Samples used

Table B4. Surface NO_x observations to model comparison, nighttime (18:00-9:00) (ppbv).

	OS2.5km	OS1km	OS1km ^{A9}	OS1km ^{B9}	OS2.5km ^{B9}	OS1km ^{B49}
IoA	-0.016	-0.050	-0.045	0.275	0.511	0.587
R	0.113	0.081	0.083	0.118	0.240	0.295
NMGE	1.913	1.982	1.971	1.366	0.920	0.777
MGE	17.235	17.858	17.756	12.306	8.291	7.004
CoE	-1.032	-1.105	-1.093	-0.451	0.023	0.174
RMSE	35.003	44.669	43.972	32.797	18.475	16.875
NMB	0.958	0.988	0.990	0.458	0.126	0.039
MB	8.634	8.899	8.915	4.124	1.139	0.350

• 1862 Samples used

Table B5. Surface O₃ observations to model comparison, daytime (9:00-18:00) (ppbv).

	OS2.5km	OS1km	OS1km ^{A9}	OS1km ^{B9}	OS2.5km ^{B9}	OS1km ^{B49}
IoA	0.141	0.192	0.184	0.338	0.396	0.529
r	0.166	0.215	0.211	0.327	0.367	0.504
NMGE	0.660	0.621	0.627	0.508	0.464	0.361
MGE	14.427	13.568	13.703	11.111	10.143	7.901
CoE	-0.718	-0.616	-0.632	-0.323	-0.208	0.059
RMSE	21.209	20.063	20.035	16.714	15.140	12.466
NMB	0.587	0.542	0.557	0.454	0.414	0.326
MB	12.839	11.854	12.187	9.918	9.050	7.121

• 864 Samples used

Table B6. Surface O₃ observations to model comparison, nighttime (18:00 to 9:00) (ppbv).

	OS2.5km	OS1km	OS1km ^{A9}	OS1km ^{B9}	OS2.5km ^{B9}	OS1km ^{B49}
IoA	0.451	0.398	0.399	0.534	0.719	0.727
r	0.526	0.541	0.557	0.642	0.784	0.784
NMGE	0.706	0.775	0.773	0.600	0.361	0.352
MGE	8.326	9.132	9.116	7.070	4.258	4.145
CoE	-0.097	-0.203	-0.201	0.068	0.439	0.454
RMSE	11.236	12.029	11.974	10.297	6.935	7.137
NMB	0.492	0.624	0.651	0.510	0.262	0.296
MB	5.799	7.359	7.668	6.008	3.088	3.491

• 1247 Samples used

Table B7. Surface PM_{2.5} observations to model comparison, daytime (9:00-18:00) ($\mu\text{g m}^{-3}$).

	OS2.5km	OS1km	OS1km ^{A9}	OS1km ^{B9}	OS2.5km ^{B9}	OS1km ^{B49}
IoA	0.372	0.356	0.364	0.495	0.555	0.625
r	0.232	0.244	0.245	0.350	0.387	0.493
NMGE	0.816	0.837	0.827	0.657	0.579	0.487
MGE	5.470	5.608	5.542	4.402	3.879	3.266
CoE	-0.256	-0.288	-0.272	-0.011	0.109	0.250
RMSE	9.607	10.312	10.034	8.059	7.286	6.626
NMB	-0.189	-0.152	-0.166	-0.231	-0.281	-0.258
MB	-1.264	-1.016	-1.109	-1.546	-1.881	-1.726

- 1862 Samples used

Table B8. Surface PM_{2.5} observations to model comparison, nighttime (18:00 to 9:00) ($\mu\text{g m}^{-3}$)

	OS2.5km	OS1km	OS1km ^{A9}	OS1km ^{B9}	OS2.5km ^{B9}	OS1km ^{B49}
IoA	0.193	0.170	0.173	0.337	0.471	0.528
r	0.163	0.183	0.178	0.277	0.368	0.442
NMGE	0.782	0.804	0.801	0.642	0.512	0.457
MGE	5.313	5.466	5.444	4.367	3.483	3.105
CoE	-0.614	-0.660	-0.653	-0.326	-0.058	0.057
RMSE	7.467	7.841	7.834	6.542	5.373	5.032
NMB	-0.293	-0.302	-0.293	-0.309	-0.293	-0.294
MB	-1.992	-2.050	-1.989	-2.098	-1.991	-1.995

- Samples used